PHOTOCHEMICAL FATE OF EMERGING POLLUTANTS IN THE URBANIZED RIVER: EFFECTS OF ANTROPOGENIC AND NATURAL WATER COMPONENTS

by

Müge Nigdeli

Integrated B.S. and M.S. Program in Teaching Physics, Boğaziçi University, 2016

Submitted to the Institute of Environmental Sciences

in partial fulfilment of the requirements for the degree of

Master of Science

in

Environmental Sciences

Boğaziçi University

2020

ACKNOWLEDGEMENTS

I would like to express my gratitude to my advisor Prof. Dr. Işıl Balcıoğlu. Without her valuable support, comments, persistent help and guidance this dissertation would not have been possible.

I am also thankful to my jury members Assoc. Prof. Dr. Başak Güven and Assoc. Prof. Dr. Gülşen Akın Evingür from Piri Reis University for their valuable supports, suggestions and kindness.

I am also very thankful to Dr. Asu Ziylan Yavaş and Technician Filiz Ayılmaz for her help and assistance in the laboratory studies done in the thesis. I also want to say thank you to Dr. Vedat Esen from Arel University for his help during process of solar simulator design.

I would like to thank all my friends in the Institute of Environmental Sciences, especially to and Fatma Büşra Yaman, Öykü Sefiloğlu and Merve Ayaz for their friendships and help in the lab

Finally, special thanks to my mother, father and husband, for standing behind me with their endless support, care and love.

ABSTRACT

PHOTOCHEMICAL FATE OF EMERGING POLLUTANTS IN THE URBANIZED RIVER: EFFECTS OF ANTROPOGENIC AND NATURAL WATER COMPONENTS

Emerging contaminants (ECs) in freshwater ecosystems are increasing with urbanization. Although some of ECs are listed as specific pollutants according to the European Water Framework Directive, there is relatively little information on the photochemical fate of various ECs. In this study, simultaneous degradation of six model ECs was investigated in both synthetic solution and Ergene River water samples by exposing them to the simulated solar light. This study was not only focused on the photodegradation of spiked ECs to the river water, but also the contaminants already found in river water. The laboratory experiments were conducted in a way to explore the direct and indirect photolysis pathway. To clarify the effects of water components on the photodegradation kinetics of model ECs in eight river water samples, which were obtained from the region far away from industrial activities, but close to the agricultural and residential activities, were characterized with organic and inorganic parameters. The detected ECs, which were four industrial pollutants and two pesticides in the river water samples regardless of the sampling site, were persistent to photodegradation while the complete degradation of ciprofloxacin, clothianidin, imazamox, imidacloprid, tetracycline and triclosan spiked at 100 mg L^{-1} concentration was achieved within 300 min irradiation time with 1360 W m^{-2} light intensity even in the water matrix receiving the effluent of a wastewater treatment plant. Direct photolysis was a significant pathway for ciprofloxacin, tetracycline and triclosan. The different optical properties both river water samples and ECs have the contribution on their photodegradation rate constants.

ÖZET

MİKROKİRLETİCİLERİN ŞEHİRLEŞMİŞ NEHİRDEKİ FOTOKİMYASAL AKIBETİ: ANTROPOJENİK VE DOĞAL SU BİLEŞENLERİNİN ETKİLERİ

Kentleşme ile tatlı su ekosistemlerinde ortaya çıkan mikrokirleticiler (EC) artmaktadır. Bazı EC'ler Avrupa Su Çevre Direktifi'ne göre spesifik kirleticiler olarak listelenmesine rağmen, çeşitli EC'larin fotokimyasal akıbeti hakkında nispeten az bilgi bulunmaktadır. Bu çalışmada, altı model EC'nin hem sentetik çözelti hem de Ergene Nehri su örneklerinde simüle edilmiş güneş ışığına maruz bırakılarak eş zamanlı bozulması araştırılmıştır. Bu çalışma sadece seçili EC'lerin nehir suyuna fotodegradasyonuna değil, aynı zamanda nehir suyunda bulunan kirleticilere de odaklanmıştır. Laboratuar deneyleri, doğrudan ve dolaylı fotoliz yolunu açığa çıkaracak şekilde gerçekleştirilmiştir. Su bileşenlerinin, model EC'lerin fotodegradasyon kinetiği üzerindeki etkilerini açıklığa kavuşturmak için, endüstriyel faaliyetlerden uzak, ancak tarımsal ve konut faaliyetlerine yakın olan bölgeden elde edilen sekiz nehir suyu örneği, organik ve inorganik parametrelerle karakterize edilmiştir. Numune alma alanından bağımsız olarak elde edilen nehir suyu örneklerinde EC olarak dört endüstriyel kirletici ve iki pestisit elde edilmiştir, ki bunlar fotodegredasyona dirençlidirler, ancak bir atık su arıtma tesisinin atık suyunu alan su matrisinde de 100 mg L^{-1} konsantrasyonda siprofloksasin, clothianidin, imazamoks, imidakloprid, tetrasiklin ve triklosan 1360 W m^{-2} ışık yoğunluğu ile 300 dakikalık ışınlama süresi içinde tamamen bozunmuştur. Doğrudan fotoliz, siprofloksasin, tetrasiklin ve triklosan için önemli bir yoldur. Hem nehir suyu numunelerinin hem de EC'larin farklı optik özellikleri, fotodegradasyon hızı sabitlerine katkıda bulunmuştur.

TABLE OF CONTENTS

LIST OF FIGURES

LIST OF TABLES

LIST OF SYMBOLS/ABBREVIATIONS

Symbol	Explanation	Unit
h	frequency	s^{-1}
m	mass	g
k	reaction rate constant	min^{-1}
Q1	parent compound	m/z
Q3	daughter compound	m/z
RT	retention time	min
t	time	min
$t_{1/2}$	half-life	min
a	absorption coefficient	m^{-1}
λ	wavelength	nm
L	path length	m^{-1}
$S_{275-295}$	spectral slope (λ=275-295 nm)	nm^{-1}
$S_{350-400}$	spectral slope (λ=350-400 nm)	nm^{-1}
sr	square radiance	
S_R	spectral slope ratio	
R^2	regression coefficient	
A	absorbance	
M	molecular structure of a pollutant	
M^*	an excited state molecule	
Al	aluminum	
Ba	barium	
Cu	copper	
Fe	iron	
K	potassium	
Mg	magnesium	
Na	sodium	
Pb	potassium	
Zn	zinc	

Abbreviation	Explanation
4-MeBT	4-Methyl-1H-benzotriazole
5-MeBT	5-Methyl-1H-benzotriazole
ACN	Acetonitrile
BS	Benzenesulfonamide
CDOM	Chromophoric Dissolved Organic Matter
CE	Collision Energy
CIP	Ciprofloxacin
CEC	Contaminants of Emerging Concern
CLO	Clothianidin
CUR	Curtain Gas
CXP	Collusion Cell Exit Potential
DOC	Dissolved Organic Carbon
DOM	Dissolved Organic Matter
DP	Declustering Potential
DPA	Diphenylamine
EC	Emerging Contaminant
EHMC	Ethylhexylmethoxycinnamate
EP	Entrance Potential
ESI	Electrospray Ionization
FA	Formic Acid
GS1	Ion Source Gas 1
GS2	Ion Source Gas 2
HMMM	Hexa(methoxymethyl)melamine
HO•	Hydroxyl Radical
ICP-OES	Inductively Coupled Plasma Optical Emission Spectrometry
IMA	Imazamox
IMI	Imidacloprid
IS	Ion Spray Voltage
LC	Liquid Chromatography
LC-ESI-MS/MS	Liquid Chromatography with Electrospray Ionization Tandem Mass Spectrometry
LOD	Limit of Detection
LOQ	Limit of Quantification

MC	Mepiquat chloride
MeOH	Methanol
ML	Molinate
MRM	Multiple Reaction Monitoring Mode
PAH	Polycyclic Aromatic Hydrocarbons
PCP	Personal Care Products
pKa	Acid Dissociation Constant
Q1	Parent Ion
Q2	Collusion Cell
Q3	Fragment Ion
RSD	Relative Standard Deviation
Rt	Retention Time
ROS	Reactive Species
TBEP	Tris(2-butoxyethyl) phosphate
TC	Tetracycline
TEM	Temperature
TET	Tetracycline HCI
TP	Total Phosphous
TRI	Triclosan
SUVA	Specific Ultraviolet Absorbance
UV-vis	Ultraviolet-visible

1. INTRODUCTION

A broad range of emerging contaminants (ECs) in aquatic environment has been a worldwide concern for many years (Arıkan et al., 2008; Bu et al., 2013; Gothwal and Shashidhar, 2015; Meffe and de Bustamante, 2014; Pal et al., 2010). The reason why they have scientific attention is that their dramatic effects on the environment, biodiversity, wildlife, and human health. It is known that conventional wastewater treatment processes are incapable of the removal of many ECs (Fairbairn et al., 2016; Jim et al., 2006; Jurado et al., 2012). Consequently, urban and industrial wastewater treatment plant effluents can be the sources of surface water pollution. However, agricultural activities can also have a contribution for the presence of ECs in the aquatic environment. Therefore, it is clear that the types and concentrations of ECs can exhibit wide variation and there is a requirement to know the fate processes of these ECs in order to evaluate their possible consequences on water resources. The physical, chemical, and biological fate processes of ECs can be responsible for the variation of their residual concentration in water bodies. Photochemical reaction can be a crucial fate process causing the transformation and degradation of ECs which are resistant to biodegradation.

In literature, there are many researches focused on the photochemical fate of ECs discharged to rivers via treated wastewater effluent (Guillet et al., 2019), on the role of effluent organic matter for the photochemical degradation of ECs (Bodhipaksha et al., 2017; Batista et al., 2016), and on the modelling of the photochemical fate of ECs in river and estuarine water (Noutsopoulos et al., 2019; Zhou et al., 2018). However, in these studies the number of ECs is limited. Moreover, simultaneous photolysis of pollutants belonging to different groups has not been studied, instead those from one group are usually targeted. The research for the fate of antibiotics is rising hot topic of recent literature. Nevertheless, surface waters contain the cocktail of contaminants and the degradation of pesticides or fate of pesticides in agricultural areas is not fully explored yet in complex matrix of surface water.

In this research, photochemical fate of a mixture of ECs including three pesticides (imazamox, imidacloprid, clothianidin), two antibiotics (ciprofloxacin and tetracycline) and one antibacterial agent (triclosan) was investigated. These chemical compounds were selected as target pollutants based on the results of a previous research project carried on the occurrence of micropollutants in Ergene River (Tezel et al., 2019) and their photolysis tendencies. The previous project made it clear

that various ECs were found in Ergene River exposed to severe pollution and the concentrations of ECs exhibit variation depending largely on the location. The variation of water matrix components can be important to evaluate the photochemical fate of ECs since organic and the inorganic constituents of river water can promote (Burrows et al., 2002; Remucal, 2014; Boreen et al., 2003; De Laurentiis et al., 2014) or inhibit the photolysis rate of pollutants (De la Cruz et al., 2012). Therefore, eight different water samples taken from Ergene River were used in this thesis and the spectroscopic properties as well as organic and inorganic constituents of the river water samples were investigated to evaluate the results of photolysis experiments performed with laboratory experiments in which the water samples were exposed to simulated solar irradiation. The achieved results in different water matrices were compared with first order degradation rate constant of each spiked ECs.

2. LITERATURE REVIEW

2.1. Occurrence of Emerging Contaminants in Aquatic Environment

Emerging contaminants or also known as contaminants of emerging concern (CECs) refer to natural or synthetic chemicals or any microorganisms that had not been detected or were not found at significant levels in the environment previously. However, ECs have potential adverse effects on wildlife and human health due to their undetermined occurring, fate, and effects (Brooks et al., 2008; Rosenfeld and Feng, 2011).

Emerging contaminants in aquatic environment have been a global common threat. The effects of ECs can be dramatic towards on the human and environmental health. They can disrupt endocrine and immune system of aquatic organisms (Stasinakis and Gatidou, 2010) and cause acute and chronic toxicity (Sousa et al., 2018). As a result of low removal rate of some ECs from wastewater in treatment plant, the endocrine system of vertebrates is affected adversely (Archer et al., 2017). Besides, antibacterial drugs as ECs can cause the development of antibiotic resistance in microorganisms (Luo et al., 2014; Petrie et al., 2015). According to World Health Organization, between 8% to 65% of *E. coli*, which is associated with urinary tract infections, have resistance to one of the main ECs; ciprofloxacin, is used treat the condition (WHO, 2018).

The ECs include a wide range of compounds such as pharmaceuticals, pesticides, steroid hormones, surfactants, industrial and personal care products, and perfluorinated compounds (Rosenfeld and Feng, 2011; Stasinakis and Gatidou, 2010; Agüera et al.,2013; Wang et al., 2017). The list goes on with the new type of compounds such as gasoline additives, flame retardants, drinking water and swimming pool disinfection-by-products, nitrosamines, plasticizers, nanomaterials, artificial sweeteners, drugs of abuse, algal toxins, siloxanes, perchlorate, benzotriazoles (Agüera et al., 2013). The concentrations of ECs in surface water generally range from $\mu g\ L^{-1}$ to $ng\ L^{-1}$ that causes some challenges for their detection and quantification (Luo et al., 2014; Stasinakis and Gatidou, 2010). Recent literature on the occurrence of ECs in river water have been reviewed in this study and these are shown in Figure 2.1 and 2.2.

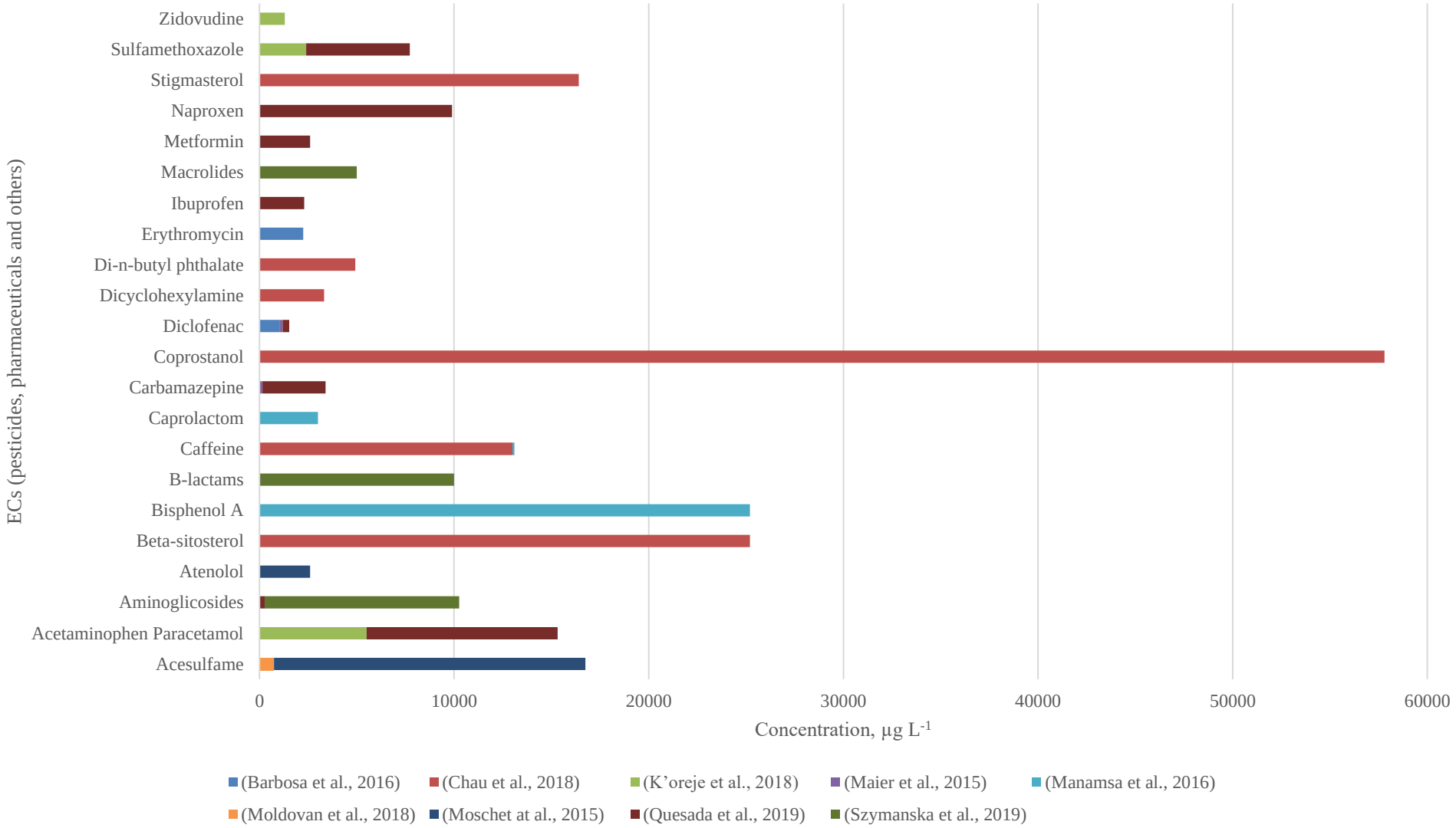

Figure 2.1. ECs found in river water.

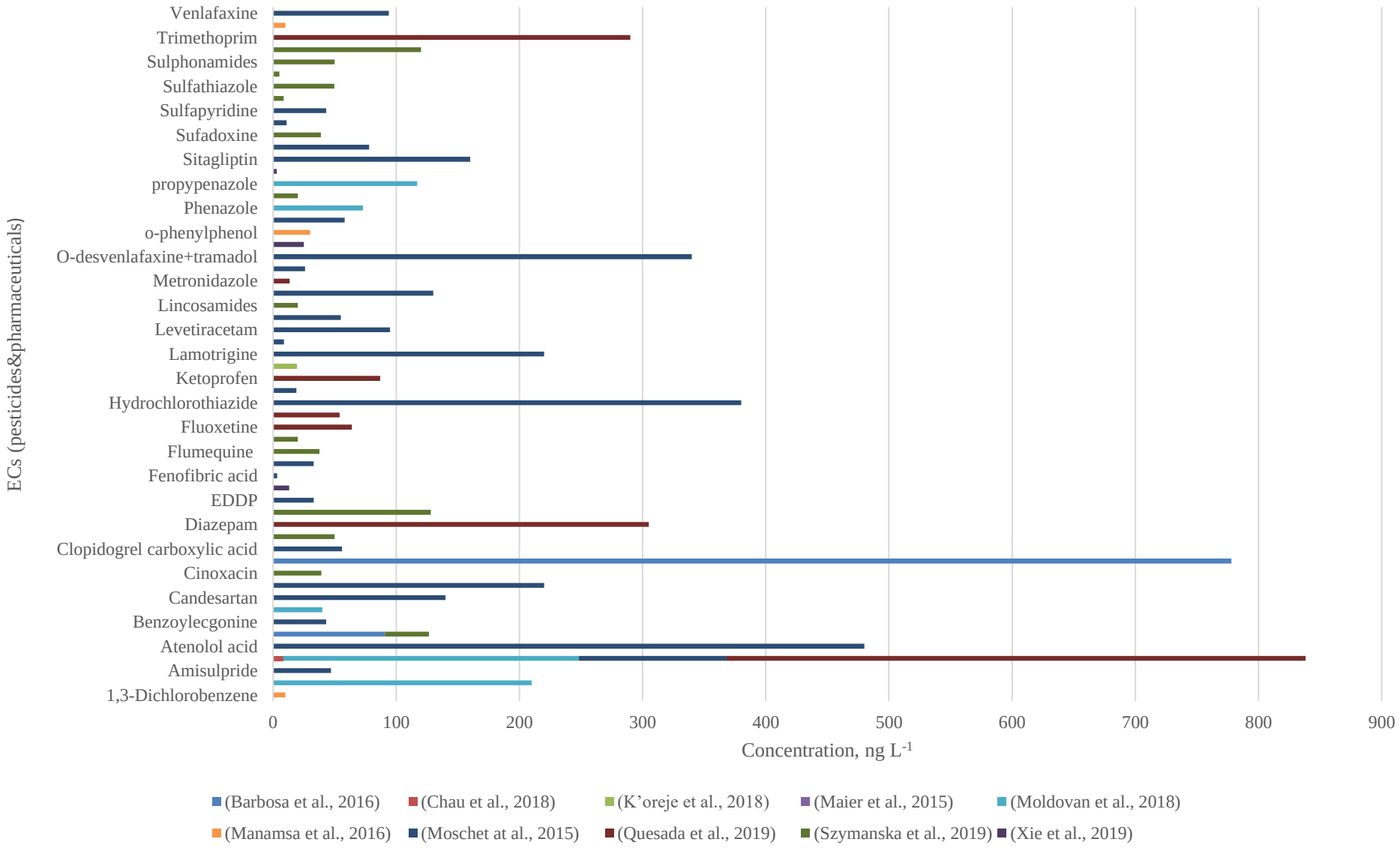

Figure 2.2. Some pesticides and pharmaceuticals found in river water.

On the other hand, in heavily polluted areas, the concentration of ECs can range up to mg L^{-1} level as revealed in a recent study in which is relevant for more than 200 pharmaceuticals were detected in river waters (Petrie et al., 2015).

Major sources of ECs in surface water are domestic, industrial and agricultural activities. The discharge of municipal and industrial wastewater effluents, leaching from landfill, urban runoff, and accidental spillage can constitute pathways for the transport of ECs into the aquatic environment (Stasinakis and Gatidou, 2010; Archer et al., 2017). However, recent studies clearly revealed that the effluents of WWTPs are important contributor for these contaminants and cause their continuous entrance into aquatic environment (Luo et al., 2014; Petrie et al., 2015). Since the WWTPs are not designed to treat a wide variety of micropollutants, which have diverse properties, ECs having recalcitrant properties cannot be eliminated in the treatment plant (Luo et al., 2014; Archer et al., 2017). Consequently, the continuous release of persistent pollutants resulted in their accumulation in the environment. ECs can experience various fate processes in the environment depending upon both intrinsic physicochemical properties of pollutant (e.g. polarity, water solubility, vapor pressure) and the environmental system in which they interact.

We need to better understand the fate of ECs in natural water resources since rapid industrialization and population growth not only result in an increase in the number of contaminants, but also elevation of their concentration levels. Sub-lethal concentrations of ECs are not well understood in environmental waters (Archer et al. 2017). The interactions of contaminant cocktail in surface waters can be significant. Their synergistic effects of ECs can be more disruptive on living organism than those exerted individually (Petrie et al., 2015). The mixture of acetaminophen, carbamazepine, gemfibrozil, and venlafaxine changes embryo production, oocyte development, and fecundity of female zebrafish, however ECs alone would not result in the same effects at the same concentrations (Archer et al., 2017). Additionally, the transformation products of ECs can be more persistent and/or toxic than the parent compound (Agüera Lopez et al., 2014; Petrie et al., 2015). For instance, under aerobic and acidic conditions, diuron, an algaecide and herbicide of the arylurea class, can be transformed into the metabolites 3,4 dichloroaniline, 1-(3,4dichlorophenyl)-3-methylurea and 1-3,4-dicholorophenylurea, which are more harmful than the parent compound (Stasinakis and Gatidou, 2010).

2.2. Fate Processes of Emerging Contaminants in Aquatic Environment

When the ECs reach environmental systems, there are multiple routes for their possible removal. The flow rate of the surface water which results in dilution, partitioning of the sediments and the particulate matter, uptake by biota, and other biotic and abiotic processes of the removal pathways of ECs (Jurado et al., 2012; Wilkinson et al., 2017). Fate processes that lead to natural elimination of pollutants can be classified as dilution, sorption, hydrolysis, biodegradation and photolysis. Figure 2.3 demonstrates the common sources and degradation pathways of ECs in the aquatic environment (Wilkinson et al., 2017).

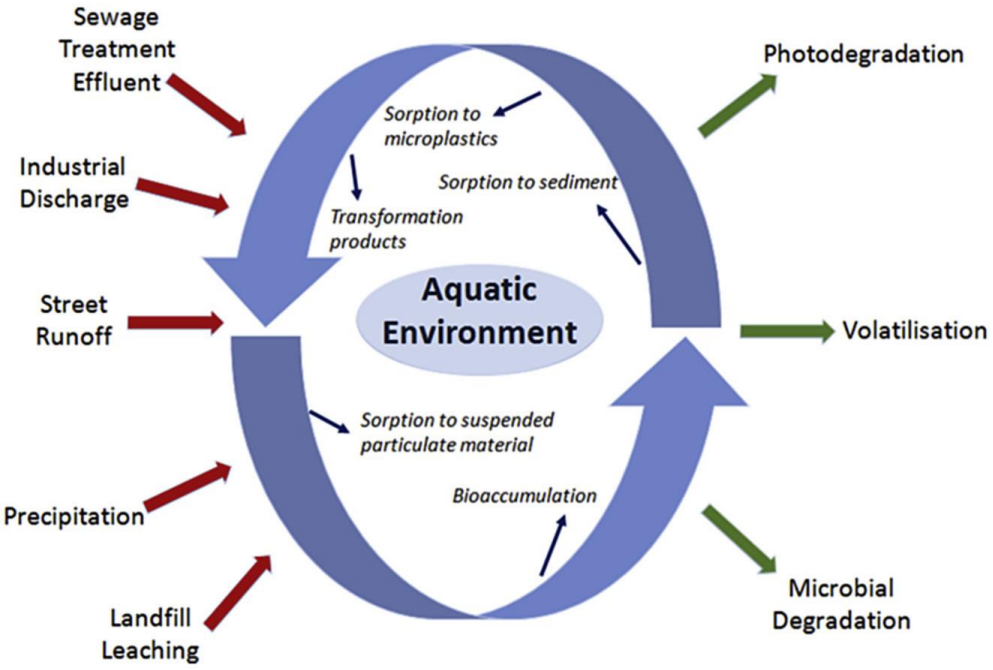

Figure 2.3. Sources and degradation pathways of ECs in aquatic environment (Wilkinson et al., 2017).

Although, biodegradation is known as one of the fate processes for the removal of pollutants from the environment, many ECs and transformation products are poorly biodegradable (Petrie et al., 2015). Moreover, some of the ECs such as antimicrobials and biocides are specifically designed to resist biological degradation (Michael et al., 2014).

Sorption of ECs to suspended particles and accumulation on sediments of river water can cause removal of some of them from aqueous phase. In addition, binding of some ECs to dissolved organic matter can contribute the removal of ECs from aqueous phase of the environmental matrix (Petrie et al., 2015).

2.3. Direct and Indirect Photolysis of Emerging Contaminants in Aquatic Environment

Photolysis is another important fate process that is responsible for the degradation or transformation of ECs in surface water. The photolysis is defined as photo induced bond breaking or rearrangement of parent molecule to form stable product(s). Organic contaminants that have certain structural moieties, such as phenol, nitro, and napthoxyl groups, can induce photochemical reactions. However, the destruction of the bonds cannot be obtained only by direct absorption of light with the chromophore group (Calza and Vione, 2015). The natural components of surface water can also absorb solar light to produce some reactive species (e.g. reactive oxygen species and photoexcited natural organic matter) that can initiate photochemical reactions of contaminants found in surface water. In this respect, photochemical reactions can be classified as direct and indirect reactions. It has been shown that photodegradation can be an important fate process for the attenuation of various pollutants including pharmaceuticals and personal care products, pesticides, textile dyes and some other commonly detected pollutants in sunlit surface waters. In Table 2.1, literature studies on the photodegradation of ECs in river water are shown together with their concentration and kinetic rate constants as a result of direct and indirect photolysis.

Table 2.1. Literature studies for the photodegradation of ECs in river water.

Contaminant	**Degradation rate constant (h^{-1}) or half-life ($t_{1/2}$)**	**Reference**
Mesotrione	k= 1.18 10^{-3} k= 0.01 with NOM and nitrate	Ter Halle and Richard, 2006
Danofloxacin *Fluvastatin* *Paroxetine*	k=187.2 k=11484 k=64.8	Santoke and Cooper, 2017
Acyclovir *Lamivudine* *Zidovudine*	k=0.05 k=0.03 k= 0.27	Zhou et al., 2015
Acesulfame	$t_{1/2}$= 3.5, 2.6, 5.1 (with 5, 10, 20 mg L^{-1} CDOM)	Gan et al., 2014
Oseltamivir carboxylate; *Oseltamivir phosphate ester*	k=0.23 k=0.05	Gonçalves et al., 2011
Sulfamethoxazole *Trimethoprim*	k=0.43 k=0.06	Ryan et al., 2011
Sulfadimethoxine	k=0.32 with Pony Lake fulvic acid k=0.23 with Suwannee River fulvic acid	Guerard et al., 2009
Clothianidin	k=0.0167 in deionized water k=0.0146 in river water	Mulligan et al., 2016
	k=0.0133 in deionized water k=0.0099 in river water	Todey et al., 2018
Ciprofloxacin	k=3.03 in canal water	Batchu et al., 2014
Imidacloprid	k=0.0286 in rice paddy water	Thuyet et al., 2011
	k=0.0119 in deionized water k=0.0089 in river water	Todey et al., 2018
Tetracycline	k=0.06 min^{-1} in river water	Śliwka-Kaszyńska et al., 2019
	k=2.271 s^{-1} in deionized water	Wei et al., 2019
Triclosan	k=0.376 in deionized water	Wang et al., 2017
	k=0.13 in surface water	Durán-Álvarez et al., 2015

As it is shown in Table 2.1, the photodegradation of danofloxacin, fluvastatin, paroxetine, ciprofloxacin and tetracycline in deionized water are more rapid than the other contaminants. For the photodegradation rate constant of ciprofloxacin, clothianidin, tetracycline and triclosan in deionized water are higher than in river water. The CDOM content in river water samples would result in competition effect during the photolysis. However, the half-life of the acesulfame increases when the CDOM content of the matrix increases. The photodegradation of the ECs would depend on their chemical properties and structure, and/or natural organic and inorganic matter in river water such as CDOM, NO_3^-.

As it is known that direct photoreaction occurs as a result of sunlight absorption by the chromophore group in the molecular structure of a pollutant (M). Depending upon the energy of absorbed light, an excited state molecule of the pollutant (M*) that is much more reactive than the parent compound can be produced. This excited state molecule undergoes physical or chemical reactions and consequently, absorbed radiation induces a particular change in the molecule in a photochemical reaction.

$$M + h\nu \rightarrow M^* \tag{2.1}$$

The light absorption by pollutants depends on their chemical structure. The chromophoric part of pollutants have the moiety of conjugated double bonds and aromatic rings which bring in a characteristic UV-vis absorption spectrum. The absorption maxima of the most pollutants results from two kinds of electron transitions: $\pi \rightarrow \pi^*$ at shorter wavelengths with intense extinction coefficient and/or $n \rightarrow \pi^*$ at longer wavelengths. Some chromophores possess conjugated double bonds that the light absorption shifts to the longer wavelengths with $\pi \rightarrow \pi^*$ transition if there is more conjugation in a molecule. The direct photolysis reactions of polycyclic aromatic hydrocarbons (PAH), haloaromatics (some pesticides), and also pharmaceuticals can be responsible for their degradation in aquatic environment. Xenobiotic compounds have special structures of aromatic rings, heteroatoms, and functional groups such as phenols, carboxyl, nitro and naphthyloxy which can absorb solar irradiation can photoreact with transient species in water (Klementova, 2018). For polycyclic aromatic compounds, the number of rings and the way the rings are fused together change the absorption spectrum. Quinolines is another type of chromophores that is able to absorb light at not only shorter wavelengths like UV light but also at longer wavelengths. Quinoid-type chromophores are also detected in natural organic matter that act as sensitizers for indirect photolysis processes. Phenols and amines are other significant type of chromophore groups that a change in their

chromophoric part in their molecular structure results in difference in their UV-vis spectrum. Deprotonation of a phenolic group leads to shift to the longer wavelengths; however, protonation of an amino group causes shrift towards shorter wavelengths (Schwarzenbach et al., 2017).

Indirect or sensitized photoreaction is occurred within two cases: the case of organic chemicals which are transformed by energy transfer via another excited species such as components of natural organic matter or the case of reaction of the organic chemicals with very reactive and short lived species such as singlet oxygen, ozone and peroxyl radicals which are formed as a result of light irradiation (Schwarzenbach et al., 2017). Indirect or sensitized photoreaction refers to the reactions occurred with very reactive, short-lived species (e.g. HO•, O_3, HO_2•, R•, ROO^-, CO_3^-•) chemically generated from the water components as a result of sunlight absorption (Leifer, 1988). It has been shown that these reactive species increase photodegradation rates of a wide variety of compounds including pesticides (Burrows et al., 2002; Remucal, 2014), pharmaceuticals (Boreen et al., 2003; Boreen et al., 2004), and personal care products (Lin and Reinhard, 2005; Kelly and Arnold, 2012; Bodrato and Vione, 2014; De Laurentiis et al., 2014). However, transient photo oxidants are found at very low concentrations in aquatic environment due to their high reactivity and these species can be easily scavenged by physical or chemical processes. The natural water components that trigger chain photochemical reactions named as photosensitizers. The main photosensitizers in surface waters are chromophoric dissolved organic matter (CDOM), nitrites (NO_2^-), nitrates (NO_3^-), and various iron (Fe(II) and Fe(III)) complexes (Schwarzenbach et al., 2017). Chromophoric dissolved organic matter (CDOM) includes aromatic amino acids, phenols, ill-defined humic substances (Nelson and Siegel, 2013). As a result of sunlight absorption first, CDOM is exited to singlet states (^{1}CDOM*) (Calza and Vione, 2015) and then energetically lower, longer-lived triplet state ^{3}CDOM* is produced. Subsequently, it can directly react with organic contaminants or generate photochemically produced reactive intermediates (Schwarzenbach et al., 2017). ^{3}CDOM* triple states oxidize water to hydroxyl radical (Vione and Chiron, 2014).

The hydroxyl radical (HO•) is one of the most powerful oxidants (Vione et al., 2018) and the most common reactive species in terms of quantity in surface waters (Han et al., 2017). The complexes between Fe(III) and organic matter have the importance as a hydroxyl radical (HO•) source; however, the main mechanism is unclear (Vione and Chiron, 2014). It is known that the production of hydroxyl radical (HO•) by Fe (II), Fe (III) and reactive iron species needs low pH values. In addition, nitrate and nitrite ions in water have an ability to form hydroxyl radicals. In many

freshwaters, the major sources for the hydroxyl radical (HO•) are shown below (Schwarzenbach et al., 2017; Ter Halle and Richard, 2006):

$$Fe^{3+} + H_2O + h\nu \rightarrow Fe^{3+} + \cdot OH \quad (2.2)$$

$$Fe(OH)^{2+} + h\nu \rightarrow Fe^{3+} + \cdot OH \quad (2.3)$$

$$NO_3^- + h\nu \rightarrow NO_3^{-*} \rightarrow NO_2^- + O\cdot^- \quad (2.4)$$

$$O\cdot^- + H_2O \rightarrow \cdot OH + OH^- \quad (2.5)$$

$$NO_2^- + h\nu \rightarrow NO_2^{-*} \rightarrow NO + O\cdot^- \quad (2.6)$$

$$\cdot OH + H_2O \rightarrow \cdot OH + OH^- \quad (2.7)$$

$$NO_3^- + h\nu + H^+ \rightarrow \cdot OH + NO_2\cdot \quad (2.8)$$

$$NO_2^- + h\nu + H^+ \rightarrow \cdot OH + NO\cdot \quad (2.9)$$

Major pathways of hydroxyl radical (HO•) when it is reacting with organic pollutants are the addition of it to a double bound or to an aromatic system or the abstraction of a hydrogen atom from a carbon atom. Many ECs including pesticides, pharmaceuticals, etc. have appreciably high reaction rate constant with hydroxyl radical (HO•) and these radical plays an important role for removal of the pollutants (Schwarzenbach et al., 2017).

The reactions of hydroxyl radical with the inorganic constituents of water can also lead to generation of long-lived, less reactive photooxidants, e.g. CO_3^{-2}• and Br^-:

$$\cdot OH + HCO_3^-/CO_3^{2-} \rightarrow CO_3^{2-} + H_2O/OH^- \quad (2.10)$$

$$\cdot OH + Br^- \rightarrow \cdot Br + OH^- \quad (2.11)$$

There are factors can have effect on the photodegradation of the emerging contaminants such as pH, wavelength of irradiance and the components of water matrix. The increase in pH of water can also increase the number of hydroxyl radical in water. As a result of this, the rate of indirect photolysis can be accelerated as shown below (Wang et al., 2017):

$$H_2O + OH^- + h\nu \rightarrow \cdot OH + H^+ + e^- \quad (2.12)$$

3. MATERIALS AND METHODS

3.1. Materials

3.1.1. Chemical Substances

4-methyl-1H-benzotriazole, 5-methyl-1H-benzotriazole (5-Tolytriazole), benzenesulfonamide, diphenylamine, ethylhexyl methoxycinnamate, hexa(methoxymethyl) melamine, mepiquat chloride, molinate, and tris(2-butoxyethyl) phosphate were target ECs that were analyzed in collected river water samples. The selection of these nine ECs was based on their non-target screening sMRM results conducted with LC-MS/MS instrument. Chemical properties and molecular structures of non-target screening contaminants are demonstrated in Appendix A. On the other hand, ciprofloxacin, clothianidin, imazamox, imidacloprid, tetracycline and triclosan were selected compounds for laboratory photolysis experiments and they were spiked to eight different river water samples. Suppliers, chemical structures and some properties of ECs are listed in Table 3.1 for spiking of river water samples and in Table 3.2 for target screening in river water samples.

The detected ECs in the sampling area at the scope of the TUBITAK project (No:115Y064) which the contaminants were used in non-target screening (Tezel et al., 2019). The stock solutions of ECs used in both target and non-target screening were individually prepared at the concentration of 1000 μg L^{-1} in methanol or in water according to their solubility and they were stored at -20°C until use. The stock solutions of all model ECs except triclosan were prepared in deionized water while triclosan was prepared in 1 M NaOH. The working solution of mixed standard used for spiking river water samples was freshly prepared at 1 mg L^{-1} in deionized water by diluting the stock solutions. Methyl-d3-triphenylphosphonium (Sigma Aldrich) was used as a surrogate standard for all analysis done with LC-MS/MS. The chemicals placed in the composition of mobile phase solution used during LC-MS/MS analysis were formic acid (HCOOH, Sigma Aldrich), methanol (CH_3OH, Merck), and water (H_2O, Merck). The LC-MS/MS properties of target and non-target ECs are listed in Table 3.3 and Table 3.4, respectively.

Table 3.1. Chemical structures and molecular properties of model ECs used for spiking of the river water samples.

Compound (Abbreviations)	Usage Area	Molecular Weight (g mol^{-1})	Molecular Formula	Molecular Structure	CAS number	Water Solubility (mg L^{-1})	Log P	Purity (%)	Supplier
Ciprofloxacin HCl (CIP)	Antibacterial drug	331.34	$C_{17}H_{18}FN_3O_3$	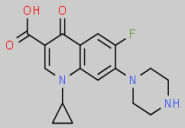	85721-33-1	30,000 (20°C)	0.28	-	MP, Biomedicals, LLC
Clothianidin (CLO)	Insecticide	249.68	$C_6H_8ClN_5O_2S$	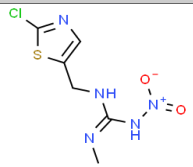	210880-92-5	327	0.7	99.4%	Bayer
Imazamox (IMA)	Herbicide	305.33	$C_{15}H_{19}N_3O_4$	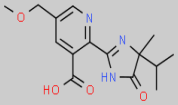	114311-32-9	4,113 (20°C)	0.73	96%	Hektaş
Imidacloprid (IMI)	Insecticide	255.66	$C_9H_{10}ClN_5O_2$	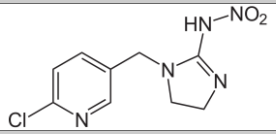	138261-41-3	31.7	0.57	97%	Hektaş
Tetracycline HCl (TET)	Antibacterial drug	444.4	$C_{22}H_{24}N_2O_8$	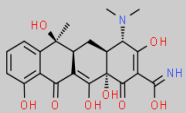	60-54-8	231 (25°C)	-1.3	95%	Sigma Aldrich
Triclosan (TRI)	Microbiocide	289.5	$C_{12}H_7Cl_3O_2$	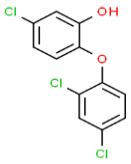	3380-34-5	10 (20°C)	4.76	97%	Sigma Aldrich

Table 3.2. Chemical structure and molecular properties of ECs used for target screening in river water samples.

Compound	Usage Area	Molecular Weight (g mol^{-1})	Molecular Formula	Molecular Structure	CAS number	Water Solubility (mg L^{-1})	Log P	Purity (%)	Supplier
4-methyl-1H-benzotriazole (4-MeBT)	Corrosion inhibitor	133.15	$C_7H_7N_3$	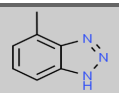	29878-31-7	1924.9	0.763	-	Sigma Aldrich
5-methyl-1H-benzotriazole (5-MeBT)	Corrosion inhibitor	133.15	$C_7H_7N_3$	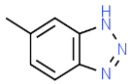	136-85-6	3069	0.974	-	Sigma Aldrich
Benzenesulfonamide (BS)	Inhibitor of human carbonic anhydrase B	157.19	$C_6H_7NO_2S$	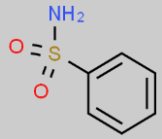	98-10-2	4300	0.31	98%	Sigma Aldrich
Diphenylamine (DPA)	Fungicide/ plant grow regulator	169.22	$C_{12}H_{11}N$	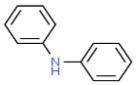	122-39-4	53 at 25°C	3.5	-	Sigma Aldrich
Ethylhexylmethoxycinnamate (EHMC)	Sunscreen	289.4	$C_{18}H_{25}O_3^-$	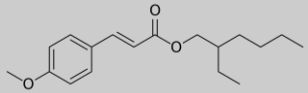	5466-77-3	0.15	5.8	-	Sigma Aldrich
Hexa(methoxymethyl)melamine (HMMM)	Collorant	390.44	$C_{15}H_{30}N_6O_6$	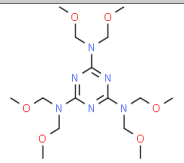	3089-11-0	149.30	0.003	-	Sigma Aldrich
Mepiquat chloride (MC)	Plant growth regulator	149.66	$C_7H_{16}ClN$	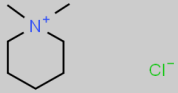	24307-26-4	9500	1.248	98%	Hektaş
Molinate (ML)	Herbicide	187.3	$C_9H_{17}NOS$	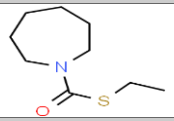	2212-67-1	970 (25°C)	3.21	97%	Hektaş
Tris(2-butoxyethyl) phosphate (TBEP)	Flame retardant	398.5	$C_{18}H_{39}O_7P$	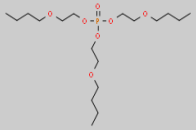	78-51-3	1100	3.75	-	Sigma Aldrich

Table 3.3. The LC-MS/MS properties of target ECs.

Compound	Q1 (m/z)	Q3 (m/z)	RT (min)	DP (V)	EP (V)	CE (V)	CXP (V)
ECs screened in river water samples							
4-Methyl-1H-benzotriazole	134.0	76.9	4.03	46	10	37	8
5-Methyl-1H-benzotriazole	134.0	77.0	4.03	56	10	33	6
Benzenesulfonamide	158.0	140.9	3.31	41	10	11	10
Diphenylamine	170.0	93.0	6.33	71	10	37	8
Ethylhexylmethoxycinnamate	291.0	161.0	8.36	51	10	27	8
Hexa(methoxymethyl)melamine	391.0	177.1	5.3	26	10	39	6
Mepiquat chloride	113.9	58.1	3.41	46	10	29	6
Molinate	188.0	126.0	6.32	51	10	19	14
Tris(2-butoxyethyl) phosphate	399.2	299.1	7.43	26	10	19	4
Model ECs spiked to river samples							
Ciprofloxacin	332.2	314.0	3.44	76	10	29	12
Clothianidin	250.0	169.1	3.81	66	10	17	15
Imazamox	306.2	261.1	4.02	76	10	31	17
Imidacloprid	256.1	175.1	3.85	71	10	29	17
Tetracycline	445.1	409.9	4.01	71	10	27	6
Triclosan	286.7	35.1	7.29	-55	-10	-28	-5

Q1 is parent compound

Q3 is daugher compound

RT is retention time

Table 3.4. LC-MS/MS properties of ECs used in non-target screening.

Emerging Contaminants	Q1 (m/z)	Q3 (m/z)	RT (min)	DP (V)	EP (V)	CE (V)	CXP (V)
1,2,3-Benzotriazole	120.0	65.0	15.00	61	10	29	8
3-Chloroaniline	128.0	92.9	15.00	51	10	25	8
4,4'-Dichlorobenzophenone	251.0	139.0	15.00	71	10	27	6
5,6-Dimethyl-H-benzotriazole monohydrate	148.1	76.9	15.00	81	10	39	6
Acetaminophen (Paracetamol)	152.0	110.0	15.00	56	10	23	8
Acetamiprid	223.1	126.0	15.00	76	10	31	11
Aclonifen	265.0	248.0	15.00	61	10	25	8
Amoxicillin	366.1	348.9	15.00	16	10	13	6
Atrazine	216.1	174.1	15.00	21	10	25	8
Azithromycin	749.5	591.3	15.00	86	10	43	6
Azoxystrobin	404.1	372.0	15.00	76	10	21	13
Benzylamine	108.1	90.9	15.00	36	10	17	6
Benzyltrimethylammonium	150.1	91.0	15.00	66	10	31	6
Boisvelone / Iso-Esuper	235.2	217.2	15.00	71	10	19	8
Cadusafos	271.1	158.9	15.00	66	10	21	13
Carbazole	168.0	167.1	15.00	76	10	51	8
Carbendazim	192.0	160.0	15.00	71	10	23	8
Clarithromycin	748.4	158.0	15.00	46	10	37	10
Di(2- ethylhexyl)phthalate (DEHP)	391.3	148.9	15.00	61	10	35	8
Diuron	233.0	71.9	15.00	61	10	41	6
Drometrizole	226.1	119.9	15.00	76	10	25	8
Epoxiconazole	330.1	120.9	15.00	81	10	31	13
Galaxolide	257.1	227.1	15.00	91	10	41	10
Metolachlor	284.1	252.0	15.00	61	10	23	23
Microcystin-RR	519.8	135.0	15.00	96	10	35	6

Table 3.4 continued

	Q1 (m/z)	Q3 (m/z)	RT (min)	DP (V)	EP (V)	CE (V)	CXP (V)
Myclobutanil	289.0	70.0	15.00	66	10	33	12
N-Benzyldimethylamine	136.1	91.0	15.00	41	10	25	6
Norfloxacin	320.2	302.0	15.00	71	10	29	12
Ofloxacin	362.2	318.0	15.00	46	10	27	6
Prochloraz	376.0	308.0	15.00	46	10	17	18
Prometryn	242.2	158.1	15.00	76	10	33	13
Prothioconazole	344.1	326.0	15.00	61	10	17	7
Quinalphos	299.0	147.0	15.00	61	10	29	14
Sulfamethoxazole	254.0	91.9	15.00	46	10	35	6
Tebuconazole	308.2	70.1	15.00	91	10	47	7
Terbutryn	242.0	186.0	15.00	61	10	27	8
Tetraacetylethylenediamine	229.1	145.1	15.00	36	10	15	8
Thiacloprid	253.2	126.0	15.00	111	12	29	14
Triphenylphosphineoxide	279.1	201.0	15.00	96	10	37	10
Methyl-d3-triphenylphophonium iodide	280.1	183	15.00	96	10	61	10

3.1.2. Sampling Campaign

River water samples were taken through the mainstream of Ergene River from its source to around Karamehmet on July 16th, 2019. Studied area is located in the northeastern of Thrace region where Ergene River stems in Saray and flow through Muratlı. The sampling locations of eight sampling points are shown on a map presented in Figure 3.1.

Figure 3.1. Satellite map showing the sampling locations on Ergene River.

Sampling point 1 (S-1) is close to location where river stems; sampling point 2 (S-2) is surrounded agricultural fields; sampling point 3 (S-3) is close to residential area; sampling point 4 (S-4) and 5 (S-5) are the locations before and after the discharging of wastewater treatment plant effluent, respectively; sampling point 6 (S-6) is the location where a tributary from agricultural area joins to main river; sampling point 7 (S-7) is junction of another tributary from rural area; sampling point 8 (S-8) is a representative location that receives domestic and agricultural wastewater. A close view of sampling locations on the satellite map is demonstrated in Figure 3.2.

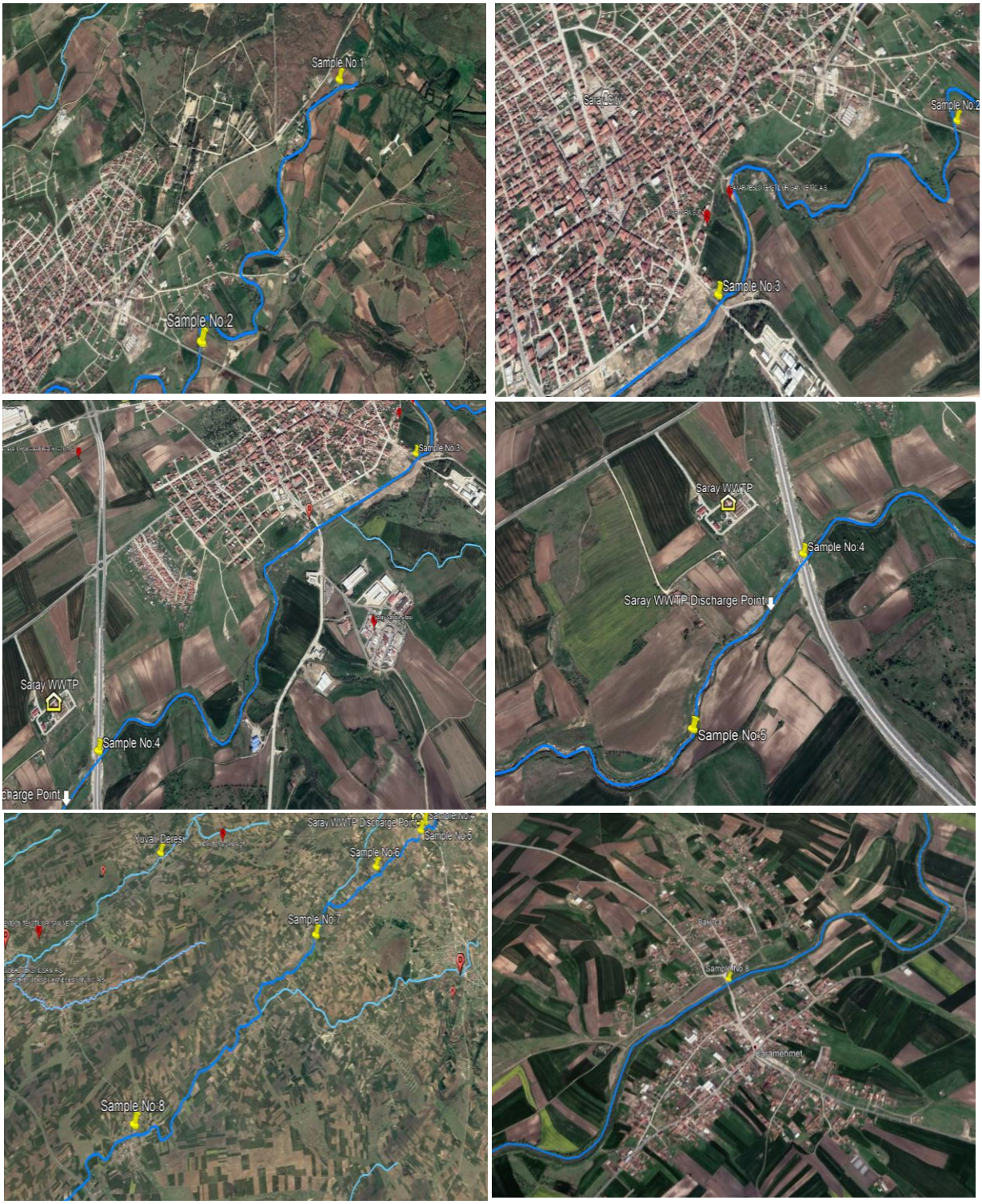

Figure 3.2. The satellite map of each sampling points.

Water samples were taken at about 10-15 cm beneath of river surface with the help of a bucket. They were filled in 1 L Teflon capped glass bottles that were rinsed previously with river water. All the samples were stored in the dark and 4°C until the characterization studies and photolysis experiments.

3.2. Methods

3.2.1. Photolysis Experiments

The laboratory scale photolysis studies were performed with an experimental set up which was specifically designed to stimulate solar light. The system was equipped with a 150-Watt Osram Xe lamp that emits light between 300-1100 nm. The intensity of the emitted light measured using a spectra photo/radiometer, Delta OHM HD 2102.1. The spectral irradiance is measured with Spectral Evolution SR 500 Laboratory Spectroradiometer. The spectra irradiance of the lamp as a function of wavelength is shown in Figure 3.3. The graph was generated using the DARwin SP Data Aquisition and Analysis Software.

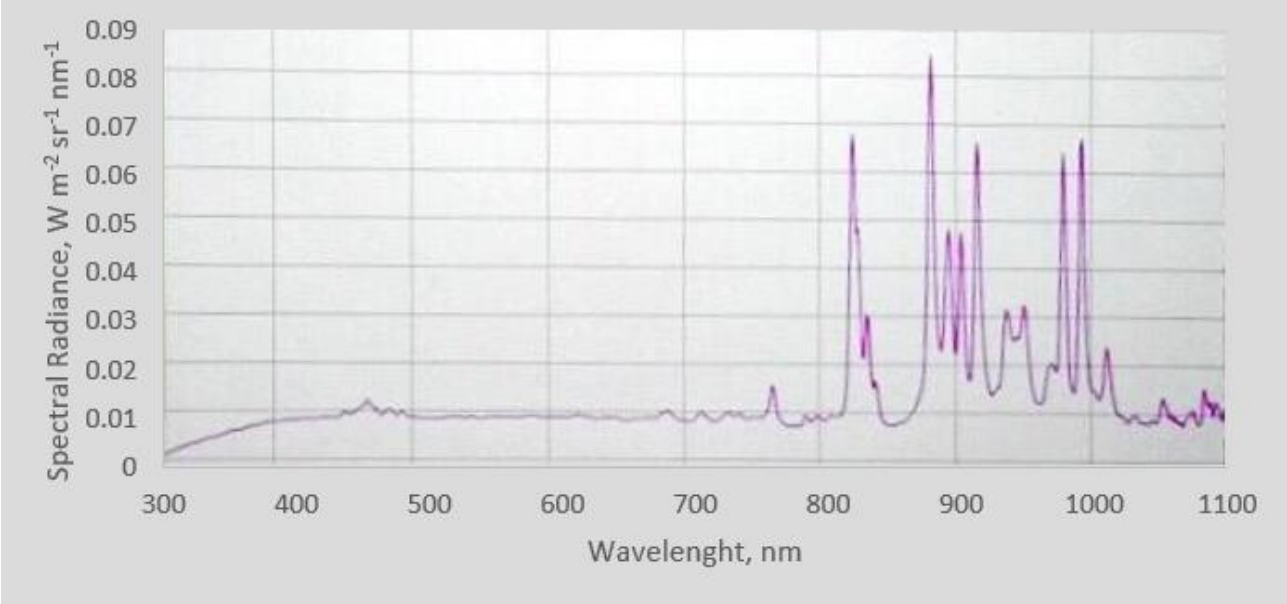

Figure 3.3. Spectral irradiance of the Xe lamp as a function of wavelength.

Teflon capped borosilicate glass tubes with a sample volume of 11 mL were used in the photolysis experiments and they were placed 30 cm below the Xe lamp in a fixed position. Ambient temperature was kept constant at 20 ± 2°C with air conditioning. Constant and continuous stirring of the samples in the tubes was enabled by an orbital shaker (Stuard SSM1) at 75 revolution per minute in order to obtain homogenization of the tube content during irradiation. The schematic representation of experimental set up is shown in Figure 3.4.

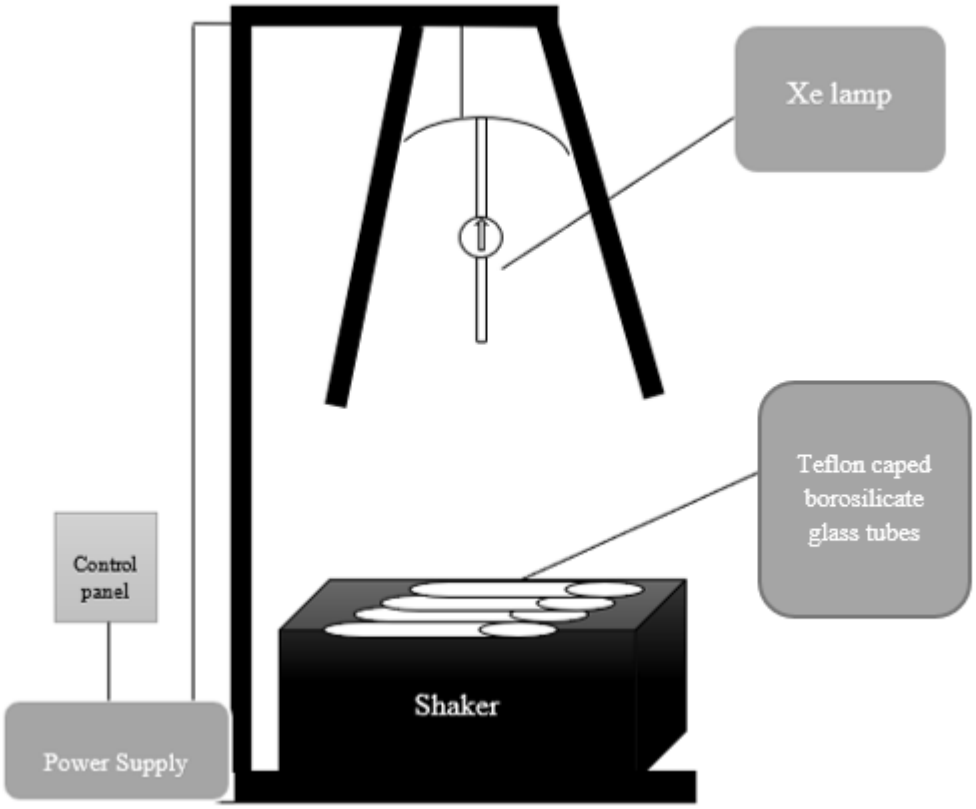

Figure 3.4. Photolysis experimental set up.

Eight different river water samples were spiked with fresh mixture of working standards of ECs. The choice of working concentrations of ECs was decided depending their occurrence in natural water systems. The aqueous samples were irradiated up to 300 min and a 100 µL aliquots of irradiated sample was taken from specified time intervals after cooling the test tube in cold water bath in five minutes. There were two types of control samples were included in photolysis experiments. Dark control experiments were conducted by covering test tubes with aluminum foil to evaluate possible losses of target ECs during the photolysis test period. Other control experiments were conducted with model ECs spiked in deionized water.

Samples are taken into 2mL amber vials were quenched by the addition of 400 µL methanol. Subsequently, 400 µL deionized water and 100 µL internal standard were added in each vial. To dilute the samples before running them for LC-MS/MS analysis considering the detection limit of the instrument. All the samples were stored at -18°C in amber vials until analysis.

3.2.2. Analytical Methods Applied to River Water Samples

The characterization of eight river water samples is performed by measuring pH, salinity, conductivity, metal content, ionic content, dissolved organic carbon (DOC), and optical properties as well as determination of ECs.

3.2.2.1. Determination of emerging contaminants. Simultaneous analyses of selected ECs were performed by using liquid chromatography with electrospray ionization tandem mass spectrometry (LC-ESI-MS/MS). Qualitative and quantitative analyses of analytes with AB SCIEX Qtrap 4500 Linear Ion Trap Tandem Mass Analyser System Coupled with Eksigent Ekspert UltraLC 110 Ultra-High-Performance Liquid Chromatography Unit were carried out at previously optimized conditions. MS/MS system was operated in multiple reaction monitoring mode (MRM). Chromatographic separations were performed on a Phenomenex Kinetex C18 (50 mm in length and 3 mm in diameter) 2.6 μm particle size column. To quantitate data and peak control, Multiquant Software was used, while for data processing and instrument control Analysis Software was used. electrospray ionization **(**ESI) probe was operated at positive ionization mode for most of the analytes; however, the separation of TRI was monitored by ESI negative mode.

MS/MS conditions with respect to the flow rate were as follows: curtain gas (CUR) is 30, temperature (TEM) is 550 °C, ion source gas 1 (GS1) is 50; ion source gas 2 (GS2) is 60. Ion spray voltage (IS) for analytes run at ESI positive mode was +5500 V, for analytes run at ESI negative mode was -4500 V. MS grade methanol and water buffered with 0.1% formic acid were used as mobile phase A and B for gradient elution, respectively. LC conditions were as follows: flow rate of mobile phase is 0.5 mL min^{-1}; temperature of the column was 40 ^{o}C; injection volume of the sample was 10 μL; total run time was 16 minutes with an initial equilibration time of 2 minutes. The gradient elution program of mobile phase is shown Table 3.5.

Table 3.5. Gradient elution program of the mobile phase.

Time	Flow Rate (mL/min)	A (%)	B (%)
0:00:01	0.50	0	100
0:01:30	0.50	0	100
0:02:00	0.50	50	50
0:04:00	0.50	50	50
0:08:01	0.50	100	0
0:14:00	0.50	100	0

As a washing solvent, methanol and acetonitrile 50:50 for pump A; and for pump B, only MS grade water was used. As a needle washing solvent, methanol and MS grade water (50:50) were used with 5% formic acid.

In this analytical technique, a triple quadrupole MS ionizes the analyte in the injected sample and separated from matrix components; subsequently fragmentation of parent ion in collusion chamber causes breaking it into its daughter ions; finally isolation of the daughter ions of each compound from each other enables quantification process in the detector. The liquid chromatography part is designed to pump the mobile phases in desired amount LC pump. The auto sampler injects liquid samples automatically under temperature-controlled conditions. The mass spectroscopy part consists of electrospray ionization, which ionized polar compound. In mass analyzer part, the ions are bombarded electrical field by ion trap analyzer which separates ions according to their mass to charge ratio (m/z) in Q1. The precursor ions experience collusion induced dissociation with high-purity nitrogen collusion gas in the collusion cell called as Q2. After collusion cell (Q2), the target analyte fragments and become daughter/product ion. In the part Q3, the ions which are high ion intensity and specification are able to transmit through detector, so the qualitative and quantitative analysis can be conducted by MS ion detector system.

3.2.2.2. Determination of inorganic water constituents. The quantitative analysis of Al, Ba, Cd, Cr, Cu, Fe, Ni, Pb, Sn, Ti, Zn analysis are conducted with atomic absorption spectroscopy using AAS, AAnalysis 300, Perkin Elmer. The Br^-, Cl^-, F^-, NO_2^-, NO_3^-, PO_4^{2-}, SO_4^{2-} content of river water samples are determined using inductively coupled plasma optical emission spectrometry (ICP-OES), Pelkin Elmer Optima, 2100 DV. The instrument was calibrated before the analytes of river water samples using 1000 mg L^{-1} certificated standard metal solution (Merck). The calibration range was between 0.05 and 0.5 mg L^{-1}. Before the analysis of Ca, Na, Mg, K, each measurement was done duplicate and the average of results were presented as mg L^{-1}.

3.2.2.3. Determination of optical properties. Optical properties of river water samples were determined with UV-Vis absorption and fluorescence spectroscopy.

UV-vis absorbance of river water samples filtered through 0.45 μm syringe filter (Millipore) was measured in a 1 cm quartz cuvette over 200 and 600 nm wavelength range with 4 nm increments against deionized water as blank on an ultraviolet-visible spectrophotometer (Unicam Helios Alpha). Samples were diluted if their DOC concentration was greater than 50 mg L^{-1}.

Absorbance units are converted to absorbance coefficients (Helms et al., 2008):

$$a_{CDOM}(\lambda) = \frac{2.303\ A(\lambda)}{L} \quad (3.1)$$

where a(λ) is absorption coefficient (m^{-1}) at wavelength λ, A(λ) is the absorbance at wavelength λ, and L is the path length (m^{-1}).

Fluorescence emission excitation matrices are recorded with each of eight river water samples diluted as needed in 1 cm quartz cuvettes using a Perkin Elmer LS 55 Fluorescence Spectrometer with a 230 voltage Xe lamp. The scanning ranges are 200-500 nm at nm intervals excitation, and 250-600 nm at nm intervals for emission with the scanning speed of 400 nm min^{-1}.

The scan application mode of the instrument is selected as synchronized delta lambda. The length of emission and excitation slits are 10nm. Scan speed is 40 nm min^{-1}. Delta lambda (Δλ) is 18 with the Δλ increment of 10 nm. Delay and delay before max are decided as 60 with the scan number of 18. Raman and Rayleigh scatter effects, inner filtering effects, instrument specific variations are all corrected during data processing. The river water samples are filtrated with 0,45 μm filter before the measurements.

3.2.2.4. Dissolved organic carbon measurement. The dissolved organic carbon analysis of for each eight river water samples was conducted on Shimadzu TOC-V CHS Total Organic Carbon Analyzer after filtration of the samples through 0.45 μm filter according to EPA DOC analysis method (Potter and Wimsatt, 2005). For DOC analysis, high temperature combustion method was used which is one of the three recommended methods of Standard Methods (APHA, 2012). Milli Q water was used as a blank during DOC analysis.

3.2.2.5. pH, conductivity, salinity, and TDS of water samples. To measure the pH values of \river water samples, WTW pH 330 was used while the measurements of conductivity, salinity and TDS measurements were carried out with WTW LF 320.

4. RESULTS AND DISCUSSION

4.1. Characterization of Collected River Water Samples

The characterization of organic matter content of the river water samples that were exposed to irradiation has been performed by LC/MS–MS, UV-vis spectroscopy, and fluorescent spectroscopy. Inorganic content of the samples was determined by the analysis of dissolved metal cations and various anions.

4.1.1. Characterization of ECs in the river water samples

To detect the number of possible ECs in eight different water samples (from S-1 to S-8) taken from Ergene River, first step of analysis was the non-target screening performed on 53 ECs in S-6 and S-8 which are more vulnerable to pollution. The types of pollutants were decided based on the results of an extensive study that was previously conducted on 300 different water samples collected from 75 sampling points located mainly downstream of the river to analyze 223 organic micropollutants (Tezel et al., 2019). Contrary to the previous study, the sampling points of this study were selected from the locations close to the source of Ergene River. Among the investigated ECs, only nine of them, namely 4-methyl-1H-benzotriazole (4-MeBT), 5-methyl-1H-benzotriazole (5-MeBT), benzenesulfonamide (BS), diphenylamine (DPA), ethylhexylmethoxycinnamate (EHMC), hexa(methoxymethyl)melamine (HMMM), mepiquat chloride (MC), molinate (ML), and tris(2-butoxyethyl) phosphate (TBPH) were detected in S-6 and S-8. The LC-MS/MS chromatograms of the S-6 and S-8 are demonstrated in Figure 4.1 a-b and Figure 4.2 a-b, respectively.

The all river water samples (from S-1 to S-8) were taken from the points which were close to agricultural and residential regions. Because agricultural activities were getting intense the sampling points with the flow of river, detection of two pesticide was expected. Although industrial wastewater was not discharged into the river in the regions where the samples were taken; the industrial pollutants, 4-MeBT, 5-MeBT, BS, HMMM, and TBPH were detected in most of the river water samples, surprisingly. Three of the ECs detected in the river water samples which are DPA, ML, and MC, classified as specific pollutants according to Environmental Quality Standards for Surface Water Resources (Orman ve Su İşleri Bakanlığı, 2016). However, the concentrations of them are not higher than the environmental equality standard values (Orman ve Su İşleri Bakanlığı, 2016).

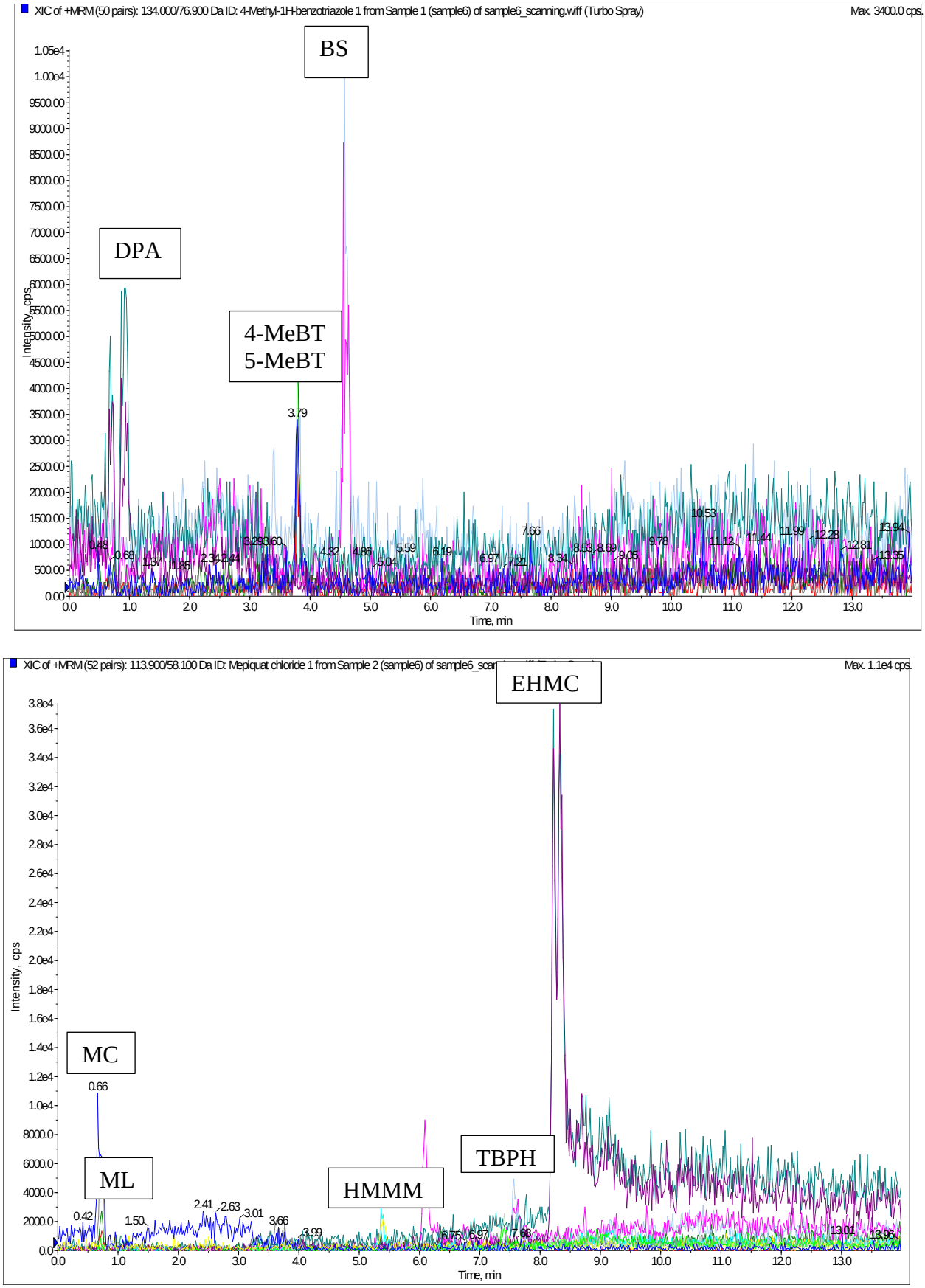

Figure 4.1. LC-MS/MS chromatogram of 4-MeBT, 5-MeBT, BS, DPA (a) and EHMC, HMMM, MC, ML, TBPH (b) in S-6.

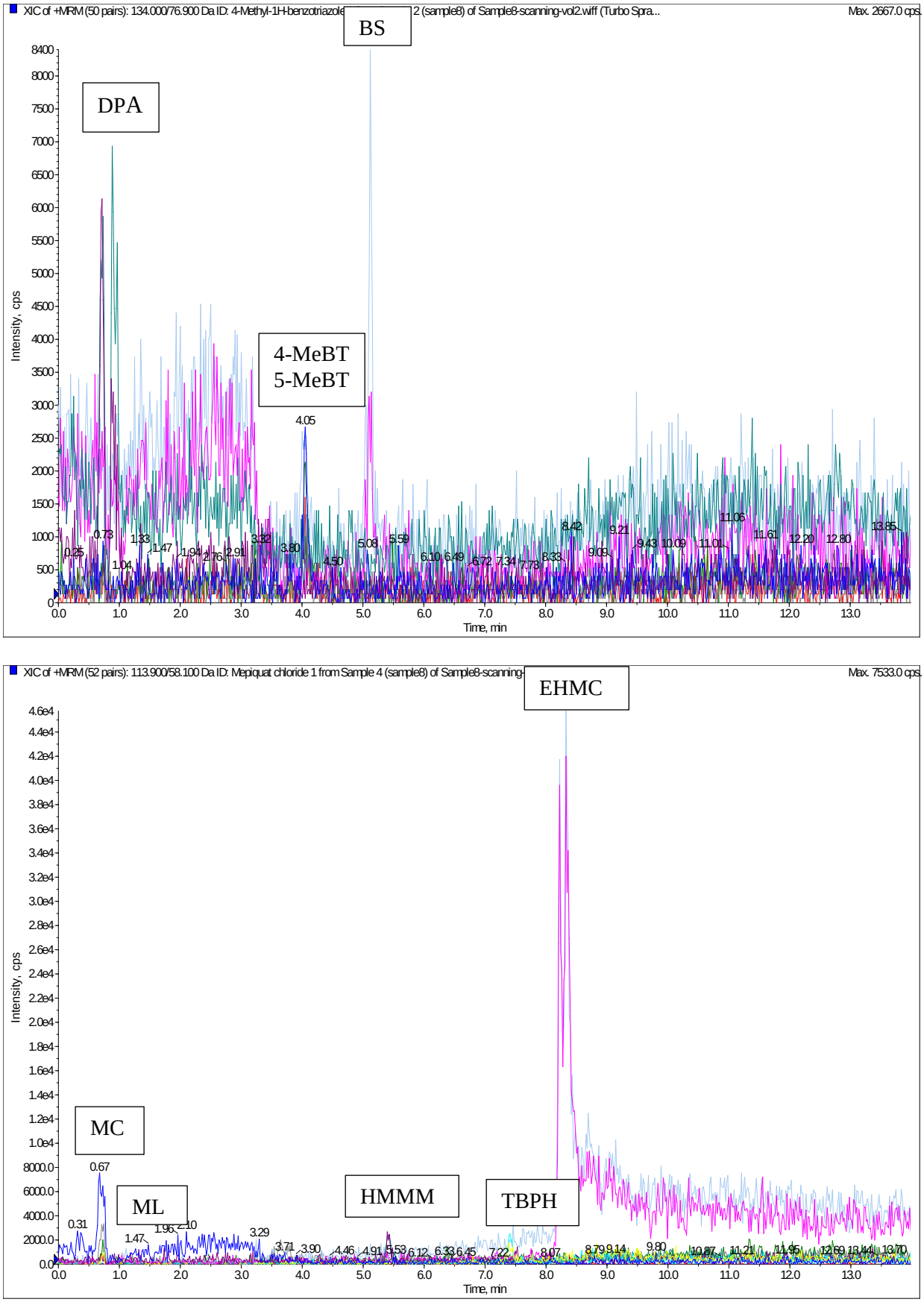

Figure 4.2. LC-MS/MS chromatogram of 4-MeBT, 5-MeBT, BS, DPA (a) and EHMC, HMMM, MC, ML, TBPH (b) in S-8.

Secondly, the quantitative analysis of the detected ECs was carried out in all river water samples in duplicate. The achieved results were evaluated according to the calibration curves of the ECs (Appendix B) that were constructed from the analytical standards in the concentration range of 1 μg L^{-1} to 100 μg L^{-1}. Table 4.1 shows mean concentrations of the detected ECs in each sampling point.

Table 4.1. Occurrence of target ECs in the river water samples.

ECs/ Samples	**S-1**	**S-2**	**S-3**	**S-4**	**S-5**	**S-6**	**S-7**	**S-8**
	Concentration (μg L^{-1})							
4-MeBT	0.059	-	-	-	0.048	0.048	0.069	0.027
5-MeBT	0.006	-	-	-	0.046	0.047	0.071	0.006
BS	14.452	5.997	8.365	7.358	29.277	23.632	23.359	35.089
DPA	4.359	5.767	-	0.276	-	-	5.524	-
EHMC	-	-	-	-	-	-	--	-
HMMM	-	-	-	-	-	-	-	163.437
MC	-	-	-	-	-	-	-	-
ML	0.023	-	17.524	15.526	0.001	0.002	0.040	-
TBPH	0.113	-	0.041	0.008	0.005	0.006	0.028	0.001

4-MeBT and 5-MeBT that are members of benzotriazoles were detected in most of the samples (S-1, S-5, S-6, S-7, and S-8) similar to the results achieved in the downstream of the river (Tezel et al., 2019) probably because of their wide use as domestic and industrial corrosion inhibitors. They are regarded as ubiquitous organic pollutants in the aquatic environment (Huntscha et al., 2014) since they are not totally removed by municipal wastewater treatment processes (Kiss and Fries, 2009; Weidauer et al., 2016). The concentration of 4-MeBT was ranged from 0.027 to 0.069 μg L^{-1} while the concentration of 5-MeBT was in the range of 0.006-0.071 μg L^{-1}. Considering the flow direction of the river and the anthropogenic activities around the sampling locations, the detection of benzotriazoles in S-1 is an unexpected result. The occurrence of these ECs at S-1 can be attributed to atmospheric deposition, and/or uncontrolled discharge (Kiss and Fries, 2009).

BS was one of the other contaminants observed in eight river samples. Benzenosulfonamides are the chemicals that have a widespread application in the production of pesticides, drugs, dyes, photochemicals and disinfectants. The concentration of this industrial compound was quite high in the river water samples and ranged from 7.358 μg L^{-1} to 35.089 μg L^{-1} while the literature data on the occurrence of this compound in surface water is in the nanogram per liter range (Herrero et al., 2013; Jover et al., 2009). The concentrations of BS in S-5, S-6, S-7, and S-8 were higher than the others.

This result could be explained by the proximity of the sampling points to residential and industrial areas. Toxic effect of this compound to aquatic organisms and bacteria has been reported (Herrero et al., 2014).

HMMM was detected only in S-8 and at extremely high concentrations (163.437 μg L^{-1}) compare to the concentrations of other ECs. As shown in Figure 3.2, S-8 receives a wastewater treatment plant effluent input. This compound that is used in the production of coatings and plastics for cans, coils, and automobiles etc. As colorant, has been detected in various surface waters in Europe (Bobeldijk et al., 2002; Dsikowitzky and Schwarzbauer, 2015; de Hoogh et al., 2006; Schwarzbauer and Ricking, 2010). The concentration of HMMM reached to around 300 000 μg L^{-1} in the downstream of the river and its presence was attributed to textile industry wastewater in the Ergene River basin (Tezel et al., 2019). Acute toxic effect to aquatic organisms and genotoxic potential to human have been reported for this compound that is resistant to biodegradation (Dsikowitzky and Schwarzbauer, 2015).

TBPH that is one of the flame retardants was found in all river water samples except S-2. Various flame retardants actually were detected at the concentrations up to 500 μg L^{-1} in the river water of Ergene Basin (Tezel et al., 2019). In literature, a growing global consumption rate of this organophosphate ester that is used as a plasticizer has been reported (He et al., 2019) although the endocrine disturbing potential of these compounds is well known (Liu et al., 2012). The concentration range of TBPH was between 0.001 and 0.041 μg L^{-1}. Surprisingly, the highest concentration of TBPH was detected in S-1 as 0.113 μg L^{-1}.

Besides the above-mentioned industrial contaminants, two different pesticides were detected in the river water samples in the study area. One of the pesticides; ML was observed in S-1 and (S-3)-(S-7) while the highest concentrations were detected in S-3 and S-4 as 17.524 μg L^{-1} and 15.526 μg L^{-1}, respectively. High agricultural input to the river water actually can be expected in these sites in the study area and this pesticide was also detected in the downstream of the river (Tezel et al. 2019). The literature data for the occurrence of ML in surface water where intensive rice crop production is performed (Silva et al., 2015) is in the concentration range of 84 ng L^{-1} and 13.64 μg L^{-1} (Silva et al., 2015).

DPA was the other pesticide detected in S-1, S-2, S-4 and S-7 which are vulnerable to agriculture input and the highest concentration was around 5 μg L^{-1}in S-2. It is known that DPA is used in fruit growing (Ingle and D'Souza, 1989) and an adverse effect on human health and long-term or short-term risk on aquatic environment have been clearly demonstrated (Tsabula et al., 2016). The occurrence of DPA at the concentration of 220.4 ng L^{-1} was reported in surface water in the literature (Robles-Molina et al., 2014).

Although EHMC and MC were identified in the water samples they were not quantified due the LOQ level of the applied analytical method. These compounds are used as a UV filter and pesticide, respectively. EHMC, which is in Watch list of European Union to monitor the surface water quality (EU Decision 2015/495), has been detected frequently in different rivers at relatively high concentrations (He, et al., 2019; Sousa et al., 2018). It is defined as slightly hazardous according to World Health Organization (Li et al., 2012).

4.1.2. Chemical characteristics of the river water samples

It is known that dissolved metal ions and inorganic anions in water can have contribution for the absorption of light in UV/Vis spectrum. Moreover, some of these ions can act as photosensitizer as well as scavenger in the photolysis process (Schwarzenbach et al., 2017). It is shown that especially nitrate (NO_3^-) and bromide (Br^-) ions which absorb light at wavelengths shorter than 240 nm can influence UV/Vis spectra of natural waters (Wozniak and Dera, 2007). Considering the influence of these constituents of water on the UV-vis spectra, the variations in concentrations of these ions have been investigated in each river water sample.

The analysis of twelve dissolved metal ions was measured in the river water samples. While cadmium (Cd), chromium (Cr), iron (Fe), nickel (Ni), tin (Sn), and titanium (Ti) ions were not able to be detected seven metal ions namely; aluminum (Al), barium (Ba), copper (Cu), potassium (K), magnesium (Mg), and sodium (Na) were detected at least one river water samples (Table 4.2). The dissolved iron (Fe), which can influence CDOM absorption measurements by forming complexes with the organics found in natural water (Xiao et al., 2013) was not detected in any sample. The concentrations of all metals in each water sample were lower than the maximum allowable limits defined by the regulation for surface water (Çevre ve Şehircilik Bakanlığı, 2004). Metal ion concentrations do not show a characteristic trend depending upon the expected inputs to the river, although there is an increase in the total metal load in river water samples with the flow of the river.

Inorganic ion content together with conductivity and pH values of the river water samples are given in Table 4.3. In overall, the concentrations of all ions and conductivity value have the lowest values at S-1 and there is an increase in these values by moving on the flow of the river. As expected around the site where the effluent of wastewater treatment plant is discharged the concentrations of ions and the conductivity have higher, an increase in nutrient concentrations can be accounted by agricultural as well as domestic activities. The nitrate (NO_3^-) that is found in the river water at concentrations range from 0.19 mg L^{-1} to 0.47 mg L^{-1} can influence the photochemical fate of ECs since this ion can act promoter or inhibitor in the direct photolysis pathway (Ge et al., 2010; Castro et al., 2017; Wang et al., 2017) A gradual increase in the concentration of F^-, Cl^-, NO_3^-, SO_4^- was also monitored along the river flow in the study area (Table 4.3). However, the concentrations of all these anions were not higher than the limits of Water Pollution Control Regulation for fresh waters (Çevre ve Şehircilik Bakanlığı, 2004).

Table 4.2. Dissolved metal ions of the river water samples.

Sample/Metal ions	Al	Ba	Cu	K	Mg	Na	Pb	Zn
	Concentration (mg L^{-1})							
S-1	0.024	0.029	0.016	1.402	2.070	10.300	0.001	0.038
S-2	0.016	0.044	0.003	6.600	2.870	13.100	0.000	0.009
S-3	0.014	0.062	0.002	6.750	3.630	19.450	0.000	0.009
S-4	0.015	0.070	0.002	5.250	4.750	34.050	0.000	0.006
S-5	0.017	0.064	0.003	6.150	0.000	38.850	0.000	0.027
S-6	0.020	0.062	0.002	6.900	4.670	39.350	0.000	0.000
S-7	0.016	0.054	0.002	5.800	4.400	29.300	0.000	0.001
S-8	0.019	0.047	0.002	6.150	4.600	30.150	0.000	0.000

Table 4.3. Inorganic ion content, conductivity and pH values of the river water samples.

Sample	F^- (mg L^{-1})	Cl^- (mg L^{-1})	Br^- (mg L^{-1})	NO_3^- (mg L^{-1})	SO_4^{-2} (mg L^{-1})	PO_4^{-2} (mg L^{-1})	Conductivity (µS cm^{-1})	pH
S-1	0.0024	0.6622	0.0000	0.1909	0.3997	0.0136	342	7.90
S-2	0.0028	0.8881	0.0000	0.2788	0.4097	0.0844	453	8.10
S-3	0.0042	1.3351	0.0100	0.2239	0.6588	0.0413	532	8.30
S-4	0.0087	2.1791	0.0122	0.1794	0.9978	0.0456	646	8.34
S-5	0.0069	2.2377	0.0116	0.2815	1.2155	0.1024	665	8.45
S-6	0.0064	2.1971	0.0114	0.3047	1.2095	0.1032	664	8.48
S-7	0.0040	1.6758	0.0111	0.4688	1.0957	0.0778	603	8.71
S-8	0.0044	1.7949	0.0098	0.4591	1.2504	0.0761	541	8.79

4.1.3 UV-Vis spectra of the river water samples

For the characterization of natural water samples dissolved organic matter (DOM) plays an important role since DOM constitutes a binding hotspot for contaminants. UV-vis spectroscopy can be used for the estimation of DOM. Chromophoric dissolved organic matter (CDOM) that is the light absorbing fraction of DOM pool can affect the optical properties of freshwater ecosystems (Ruhala and Zarnetske, 2017). This optically active fraction of DOM, CDOM can compete with the contaminants during the solar light driven fate process. In addition, this fraction can initiate photochemical mediated processes. In the study, UV/Vis absorption spectrum of each river water samples was recorded to evaluate the possible shading effect of CDOM on the photolysis of spiked ECs. The results are plotted in terms of both absorbance and natural logarithm of absorbance (absorption coefficient) versus wavelength (λ) in Figure 4.3.

The evaluation of UV/Vis spectrum for the quantification of riverine CDOM has been studied in several studies in the literature (Stedmon et al., 2000; Osburn et al., 2016). In accordance to the previous studies, UV-Vis spectra of CDOM in each river water samples exhibited a typical trend of natural water and the absorbance decreases with increasing wavelength (Helms, et al., 2008; Bricaud et al., 1981; Green and Blough, 1994). Due the overlaps of various chromophoric groups of water constituents, each spectrum is featureless in terms of well-defined maxima. However, the absorbance values of different river water samples, especially at shorter wavelength of the spectrum are considerably different (Figure 4.3). The absorption rates of S-1, S-2 and S-3 at shorter wavelengths are relatively lower than those of the other samples. This result can be attributed to the higher agricultural and domestic inputs to the river at sampling sites of (S-4)-(S-8).

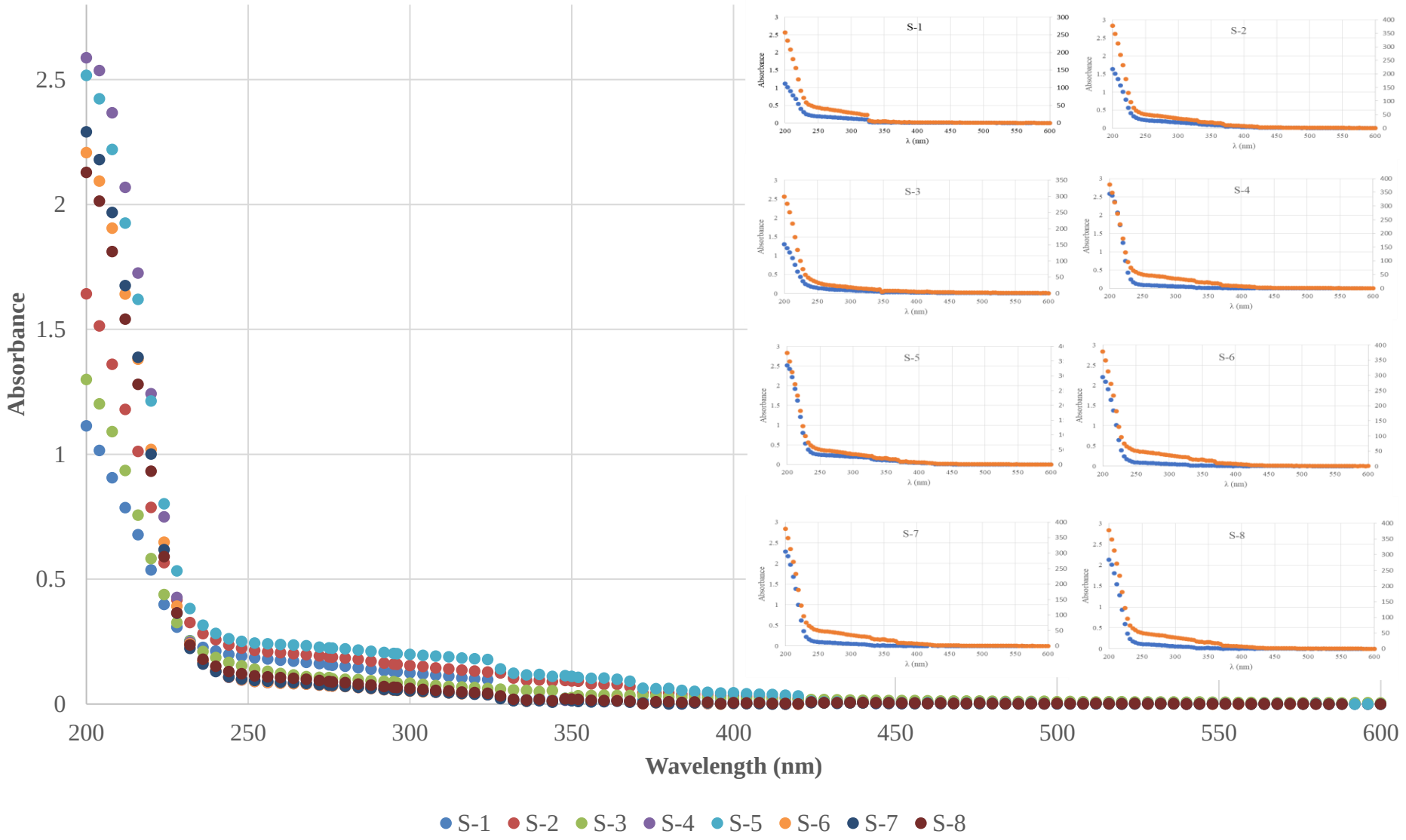

Figure 4.3. UV-Vis absorbance spectrum of eight river water samples.

4.1.4. Absorption Spectra Parameters:

Although the absorbance at single specific wavelength (e.g. 250, 254, 280 300 nm etc.) and/or absorption ratio at two different wavelengths (e.g. A_{250}/A_{365} etc.) have been used to characterize CDOM, spectral slope parameters have been successfully employed to provide information on the properties and the origin of CDOM in the literature (de Haan and de Boer 1987; Spencer et al., 2007; Helms et 2008). In this study, spectral slope (S) was calculated at two different wavelength ranges, namely 275-295 nm and 350-400 nm ($S_{275\text{-}295}$ and $S_{350\text{-}400}$) since the greatest variations in S was detected in these wavelength ranges similar to the previous literature studies (Stedmon and Nelson, 2015; Li and Hur, 2017). In addition to spectral slope parameters, specific ultraviolet absorbance ($SUVA_{254}$) was determined for each river water sample.

4.1.4.1. Spectral slope parameters. Spectral slopes, $S_{275\text{-}295}$ and $S_{350\text{-}400}$, were calculated by using an exponential model given with equation 4.1 (Kirk, 1994; Helms et al., 2008)

$$a_{CDOM(\lambda)} = a_{CDOM(\lambda_0)} e^{-S(\lambda-\lambda 0)} \qquad (4.1)$$

where $a_{CDOM(\lambda)}$ is the absorption coefficient at wavelength λ; $a_{CDOM(\lambda_0)}$ is the absorption coefficient at a reference wavelength λ_0; S is the spectral slope parameter.

MATLAB curve fitting toolbox (The MathWorks, 2018) was used for calculation spectral slope parameter by using fitted and exponential equation. The reference wavelength was determined by finding the best regression coefficient between fitted equations and experimental results.

Subsequently, spectral slope ratio (S_R) was calculated dividing $S_{275\text{-}295}$ to $S_{350\text{-}400}$ (Helms et al., 2008; Ruhala and Zarnetske, 2017):

$$S_R = S_{275-295}/S_{350-400} \qquad (4.2)$$

The S values together with correlation coefficients and S_R for each river water samples are listed in Table 4.4.

Table 4.4. Spectral slope parameters of the river water samples.

Sample	$S_{275-295}$ (nm^{-1})	$S_{350-400}$ (nm^{-1})	S_R
S-1	0.009 (0.992)	0.018 (0.748)	0.502
S-2	0.009 (0.976)	0.024 (0.933)	0.379
S-3	0.008 (0.950)	0.008 (0.924)	0.933
S-4	0.013 (0.989)	0.036 (0.721)	0.361
S-5	0.005 (0.994)	0.022 (0.932)	0.239
S-6	0.013 (0.988)	0.051 (0.834)	0.261
S-7	0.015 (0.999)	0.035 (0.777)	0.420
S-8	0.016 (0.986)	0.035 (0.810)	0.448

In literature, some hypotheses on the spectral parameters have been put forward and their validity is shown for different surface waters (Spencer et al., 2007; Helms et al., 2008; Li and Hur, 2017). Increasing conjugation in the molecular structure of CDOM, which results in larger molecular size and weight with the broadening of absorption spectra towards visible region (Stedmon and Nelson, 2015; Lei et al., 2019). The higher absorption at longer wavelengths diminishes the values of $S_{275-295}$. It was also suggested that $S_{275-295}$ values greater than 0.015 nm^{-1} refers to CDOM with low molecular weight (Shao et al., 2016). Based on the literature hypotheses, it is suggested that the content of CDOM is composed of the substances with the high molecular weight.

$S_{275-295,}$ is also used to indicate the source of DOM in terms of aquatic or terrestrial origin (Helms et al., 2008; Shao et al., 2016; Li and Hur, 2017; Zhou et al, 2019). While the steeper value of $S_{275-295}$ refers to autochthonous or aquatic source for DOM, lower value of $S_{275-295}$ is associated with terrestrial based DOM (Gao et al., 2019; Shao et al., 2016; Spencer et al., 2007). According to Helms (2008), S_R is also another indicator for the source of the CDOM in river water samples and a correlation was found between increasing S_R and decreasing terrestrially originated CDOM content. The lower values of $S_{275-295}$ compared to those of $S_{350-400}$ and S_R <1 indicated that CDOM of Ergene River in the study area has high molecular weight and terrestrially derived.

4.1.4.2. SUVA254 parameter. In order to determine aromaticity content of CDOM in river water samples, specific UV absorbance at 254 nm wavelength named as $SUVA_{254}$ parameter was calculated by normalizing the absorption coefficient to dissolved organic carbon (DOC) concentration (Helms et al., 2008; Ruhala and Zarnetske, 2017; Gao et al., 2019).

$$SUVA_{254} = \left(\frac{a_{254}}{DOC}\right) \quad (4.3)$$

where a_{254} is the absorbance coefficient at the wavelength of 254 nm wavelength and, DOC is the dissolved organic matter concentration of the river water samples. The calculated $SUVA_{254}$ for each water samples are given in Table 4.5.

Table 4.5. Specific UV absorbance of the river water samples.

Sample	A_{254}	a_{254} (m^{-1})	***DOC*** (mg L^{-1})	$SUVA_{254}$ (L mg^{-1} m^{-1})
S-1	0.183	42.030	4.415	9.520
S-2	0.212	48.824	5.803	8.414
S-3	0.136	31.206	4.644	6.720
S-4	0.088	20.266	4.712	4.300
S-5	0.243	55.848	4.524	12.345
S-6	0.089	20.382	4.712	4.326
S-7	0.183	42.030	4.620	9.097
S-8	0.183	42.030	3.909	10.752

$SUVA_{254}$ value of S-5 was different from the other river water samples. It is noteworthy that this situation is actually valid for $S_{275-295}$ and S_R values. It was mentioned that $SUVA_{254}$ is proportional to aromacity but $S_{275-295}$ and S_R are inversely proportional to aromaticity (Stedmon and Nelson, 2015). The input of WWTP effluent to the river water can cause the formation of a complex matrix.

4.1.5. Fluorescence spectra of river water samples:

The fluorescence spectra can also be used to estimate the sources of the CDOM found in river water samples. Fluorescence excitation-emission matrix (EEM) combined with parallel factor analysis (PARAFAC) would give distribution of all fluorescent components by identifying and characterizing them in a range of excitation and emission matrix. The fluorescent data of the river water samples were tested in PARAFAC modeling using DOM Fluor toolbox in MATLAB software (in the format of R2018a) (Stedmon and Bro, 2008; Stedmon and Bro, 2009; Yang et al., 2015) and the achieved results for S-1, S-4, S-5 and S-7 are given in Figure 4.4.

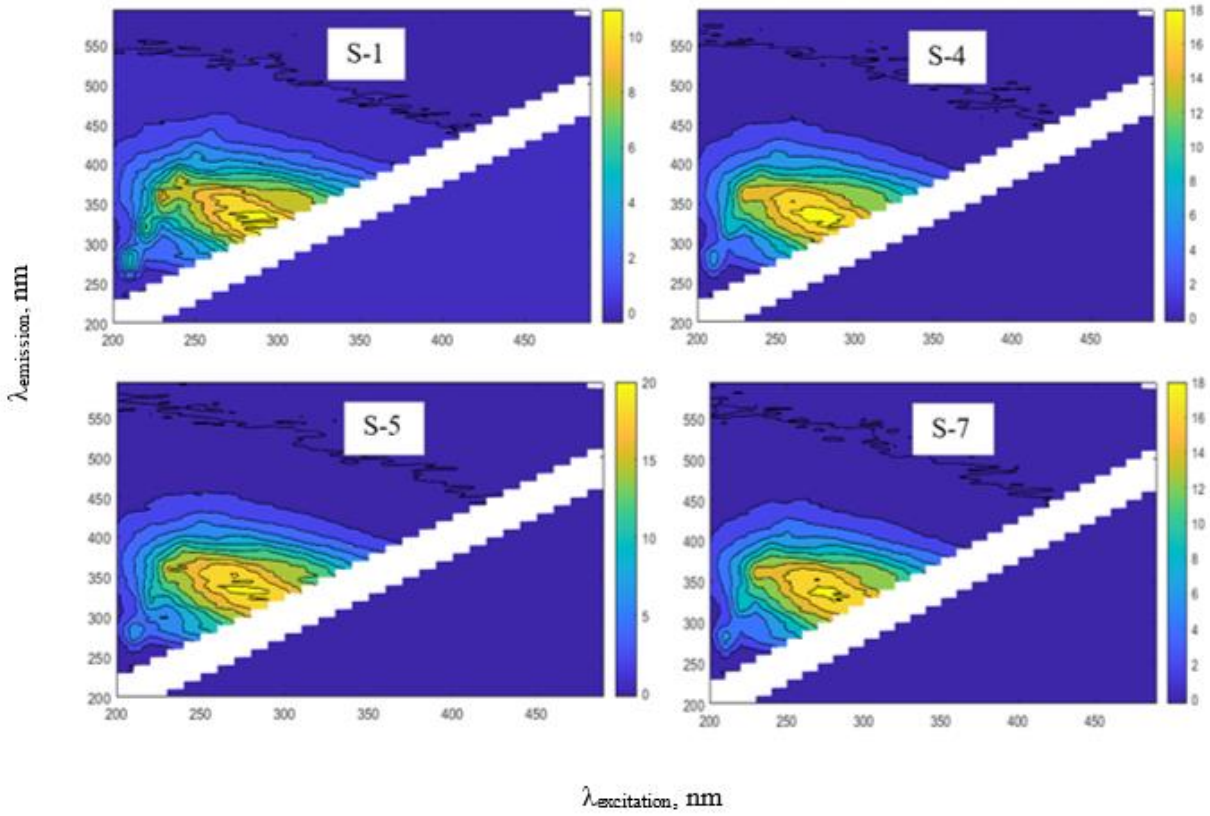

Figure 4.4. PARAFAC Analysis of EEM of samples S-1 (a), S-4 (b), S-5 (c), and S-7 (d). Legends show intensity of emission at specific excitation wavelength.

In literature, as a result of PARAFAC modeling two components termed B (fluorescence peaks at $\lambda_{Ex/Em}$: 220-280 nm/300-302 nm) and T (fluorescence peaks at $\lambda_{Ex/Em}$: 220-290 nm/349-369 nm) have been identified and the correspondence of these components to tryptophan-like and tyrosine-like peak regions of EEM have been reported, respectively (Spencer et al, 2007; Shao et al., 2016). A strong fluorescent intensity of protein-like substances has been shown in the river water polluted by anthropogenic activities including domestic and others (Shao et al, 2016; Spencer et al., 2007). The fluorescence characterization of the river water samples has shown the presence of both protein-like fluorescent structures (Figure 4.4 a-d). However, a remarkable difference has been determined between the fluorescence intensity of S-1 and S-5. This result is in accordance with the values of $SUVA_{254}$ and slope parameters.

4.2. Photodegradation of model ECs in river water samples

In this part of the study, the photodegradation of pollutants has been investigated in the river water matrices collected from the study area. Two different series of photolysis experiments have

been performed: (i) eight river water samples individually exposed to irradiation to observe the degradation of the ECs that have already been detected in (S-1)-(S-8), (ii) a mixture of six different model ECs were spiked to each of the river water samples and the simultaneous photodegradation of model ECs was monitored. In addition, the degradation of model ECs in deionized water was studied to assess direct photolysis pathway. Dark control experiments were also carried out for both the solutions of model pollutants in deionized water and in river water samples.

4.2.1. Photodegradation kinetics of ECs

The first and second series of photolysis experiments were conducted with the light intensity of 1360 W m^{-2}. In the second series of the experiments the spiking concentration of model ECs was selected as 100 μg L^{-1} considering low concentrations of ECs in the aquatic environment. The results of photolysis experiments were evaluated according to the calibration curves of the model ECs (Appendix C) that were constructed from the analytical standards in the concentration range of 1 μg L^{-1} to 100 μg L^{-1}.

As a result of the first experimental series it can be deduced that the contaminants found in the river water samples did not show any degradation during the 300 min irradiation period (data not shown). In literature, the half-life of 5-MeBT was reported as 840 min in wastewater exposed to simulated solar light (Chung et al., 2018) while the half-life of ML was determined as 62.4 d under natural sunlight in river water (Konstantinou et al., 2001). All these results can indicate the persistence of the determined ECs to photodegradation in different water bodies.

Dark control experiments performed by spiking the model ECs to the river water samples resulted in either a slight decrease or no change in their concentrations of model ECs. The concentrations of CLO, IMA, and IMI did not show a significant change over the time period of 420 min. The degradation of CIP and TET varied depending upon the water matrix. While CIP has the degradation percentage of 23-12% TET has the degradation percentage of 45-30% within 420 min in S-7 and S-8, respectively. The degradation percentage of TRI is detected at 10% in two river water samples.

The results of the second experimental series are shown Figure 4.5-4.7 in terms of normalized concentrations of each spiked ECs versus irradiation time. As shown in the figures all investigated ECs exhibited complete degradation. In order to calculate the reaction rate constant of each ECs, the first order kinetic model that is given by equations 4.4 and 4.5 was applied to experimental data:

$$\frac{dC_t}{dt} = -kC_t \quad (4.4)$$

$$k = -\ln\left(C_t/C_0\right) t \quad (4.5)$$

where, dC_t/dt is the concentration change of the compound per unit time, and k is the photodegradation rate constant ($time^{-1}$), t is time, C_0 and C_t are the concentration of the model compound at the beginning of the photolysis experiment and at time t, respectively.

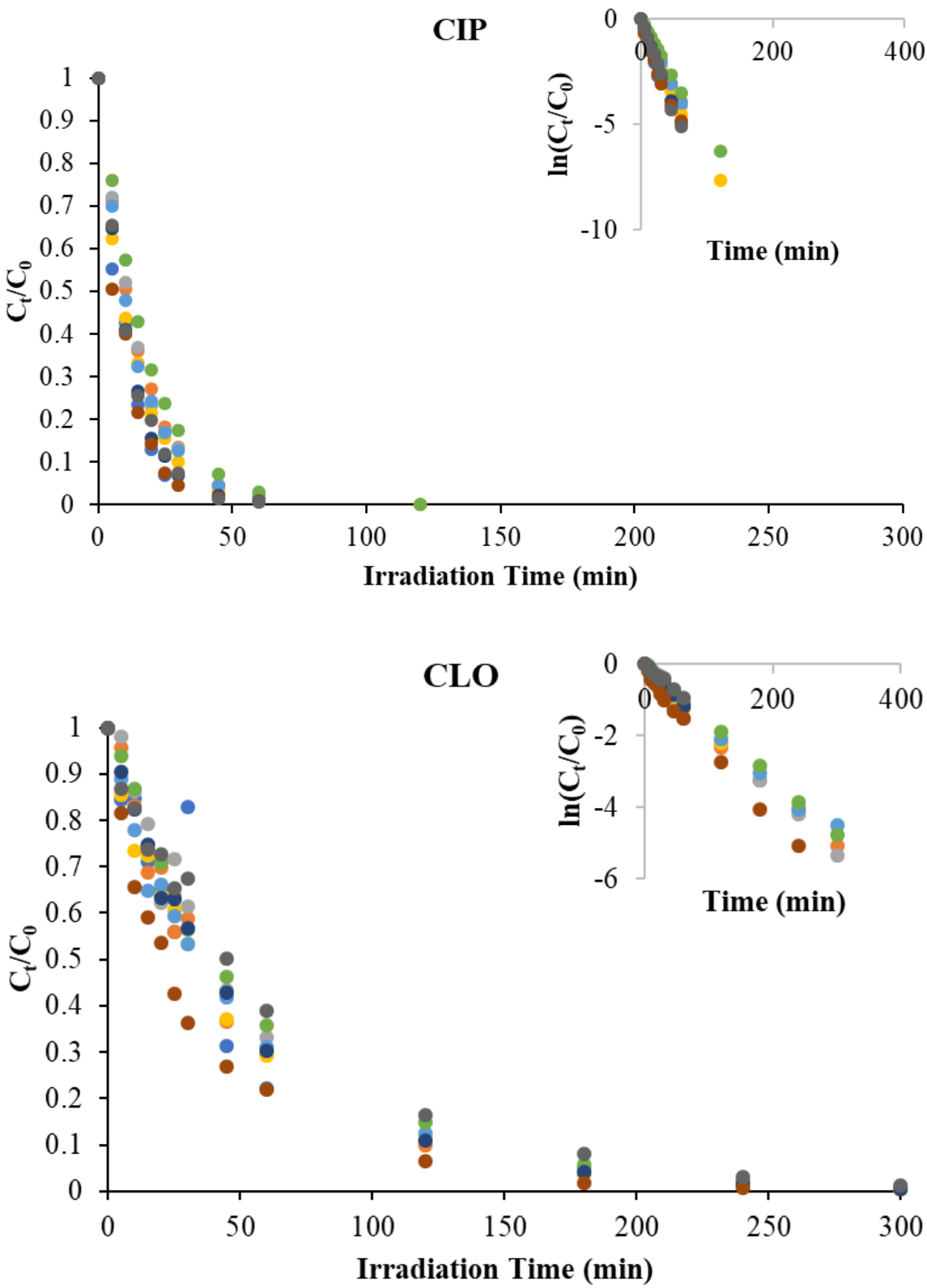

Figure 4.5. Photodegradation profiles of (a) CIP and (b) CLO spiked to the river water sample.

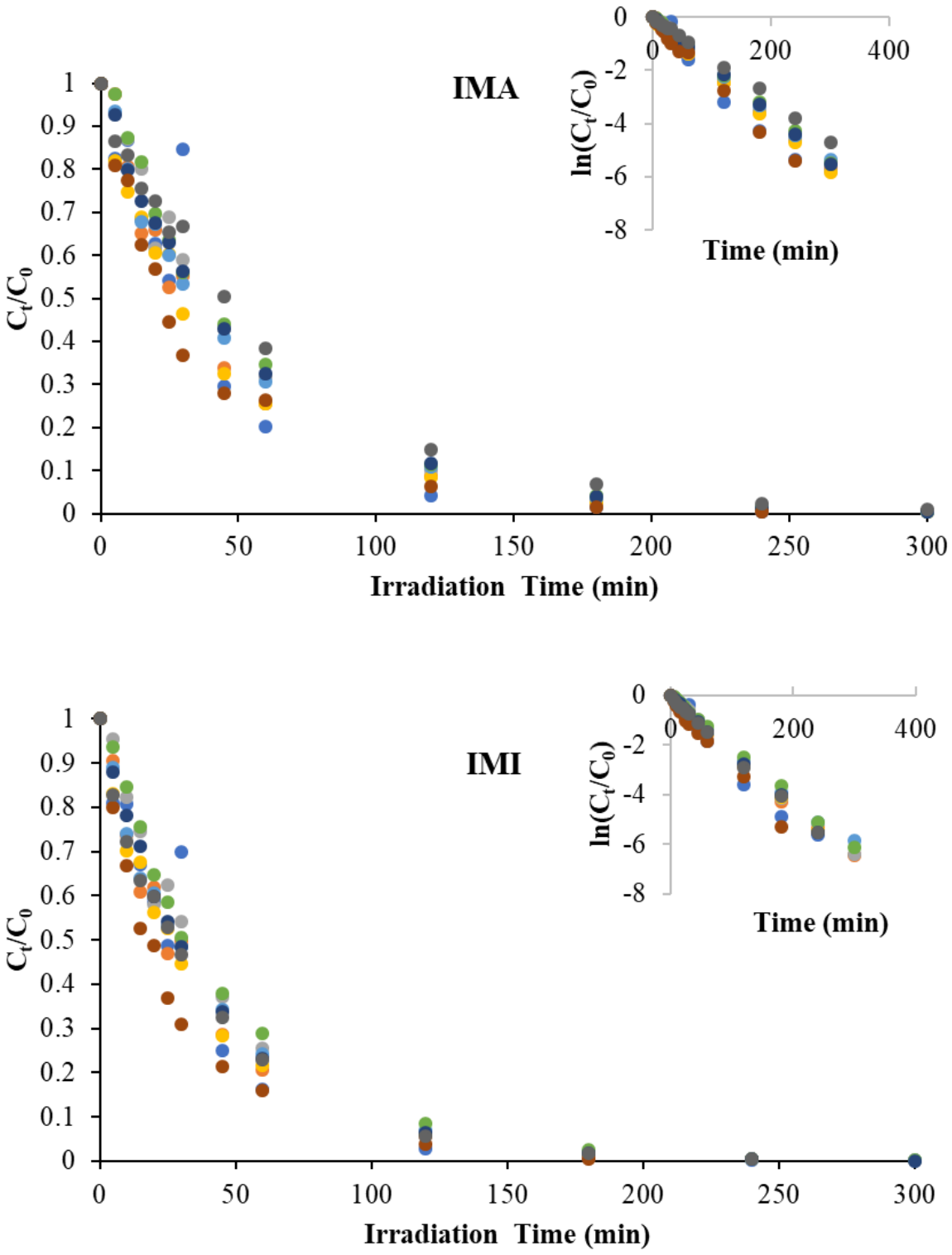

Figure 4.6. Photodegradation profiles of (a) IMA and (b) IMI spiked to the river water sample.

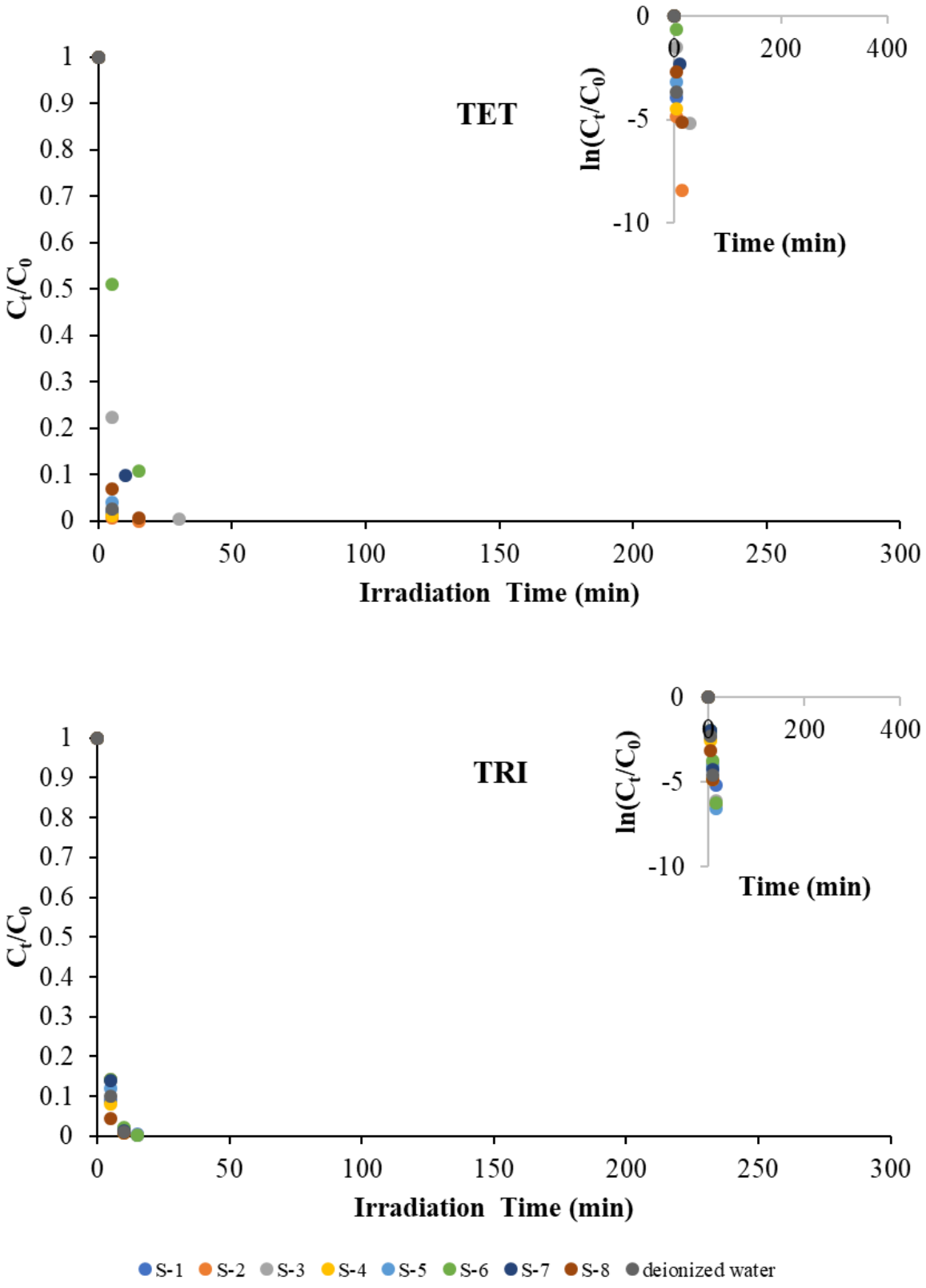

Figure 4.7. Photodegradation profiles of (a) TET and (b) TRI spiked to the river water sample.

The half-life ($t_{1/2}$) of the model compound is calculated by the following equation:

$$t_{1/2} = {\ln 2}/{k} \quad (4.6)$$

In order to find k and $t_{1/2}$ values the kinetic evaluations of each EC are shown in Figure 4.5-4.7 as an inset. As deduced from these figures, the photodegradation of all ECs fitted well to the first-order kinetic model. The kinetic reaction rate constants together with regression coefficients, and half-lives of model ECs are listed in Table 4.6 and 4.7, respectively. These tables also include the results achieved in deionized water.

Table 4.6. Photodegradation rate constants of model ECs.

	CIP	**CLO**	**IMA**	**IMI**	**TET**	**TRI**
Sample	k, min^{-1} (R^2)					
S-1	0.105 (0.989)	0.026 (0.992)	0.023 (0.983)	0.025 (0.978)	0.789 (1.000)	0.401 (0.987)
S-2	0.069 (0.997)	0.017 (0.996)	0.019 (0.997)	0.022 (0.996)	0.534 (0.926)	0.418 (0.997)
S-3	0.069 (0.997)	0.018 (0.999)	0.019 (0.999)	0.022 (0.998)	0.166 (0.984)	0.407 (0.999)
S-4	0.065 (0.990)	0.017 (0.998)	0.019 (0.998)	0.022 (0.999)	0.898 (1.000)	0.484 (0.999)
S-5	0.066 (0.998)	0.015 (0.993)	0.018 (0.999)	0.020 (0.996)	0.637 (1.000)	0.431 (0.998)
S-6	0.055 (0.998)	0.016 (0.999)	0.018 (1.000)	0.021 (0.999)	0.149 (0.999)	0.410 (0.996)
S-7	0.082 (0.997)	0.018 (1.000)	0.018 (1.000)	0.023 (0.999)	0.231 (1.000)	0.427 (0.998)
S-8	0.082 (0.978)	0.021 (0.994)	0.022 (0.995)	0.028 (0.993)	0.328 (0.954)	0.488 (0.974)
S (DI)	0.088 (0.993)	0.014 (0.999)	0.016 (0.999)	0.023 (0.999)	0.734 (1.000)	0.458 (1.000)

Table 4.7. Half-lives ($t_{1/2}$) of model ECs.

	CIP	**CLO**	**IMA**	**IMI**	**TET**	**TRI**
Sample	$t_{1/2}$ (min)					
S-1	6.620	26.660	29.749	27.615	0.878	2.007
S-2	10.046	41.015	36.481	31.796	1.298	1.657
S-3	10.104	38.941	35.729	31.364	4.183	1.703
S-4	10.746	41.259	36.101	31.083	0.772	1.432
S-5	10.439	45.010	38.508	34.657	1.088	1.608
S-6	12.695	43.870	38.295	33.648	4.646	1.692
S-7	8.422	39.383	37.877	30.535	3.005	1.623
S-8	8.432	33.485	31.083	24.933	2.113	1.421
S (DI)	7.886	49.159	44.719	30.670	0.944	1.514

The degradation rates of all ECs except TRI were faster in S-1 compared to those achieved in other river water samples and deionized water. The lack of light shading components of S-1 can explain the faster degradation of the ECs (Figure 4.3). Another observation of the results presented in Table 4.6 is the relatively lower photodegradation rate constants of the ECs in deionized water that can be attributed to indirect photolysis.

Among the investigated ECs TET, TRI, and CIP have higher degradation rate constants (Table 4.6). It should be taken in to account that instability of TET and CIP has a contribution in their degradation depending upon the results of dark control experiments. However, it is known these ECs are able to undergo direct photolysis (Ge et al., 2010; Daghrir and Drogui, 2013; Vione and Chiron, 2014; Mangalgiri and Blaney, 2017; Wei et al., 2019). The absorption spectrums of the ECs prepared in deionized water at 5 mg L^{-1} concentration were recorded in the wavelength region of 300 and 400 nm and they are shown together with the literature data in Figure 4.8, although it was mentioned that IMA only absorb light in the wavelength region of 300-400 nm (Figure 4.8). However, the degradation rate constants of IMA were comparable to those obtained for CLO that has absorption within 300-330 nm wavelength region. In addition, the degradation rate of TRI was higher than that of CIP. This result can indicate the importance of molecular reactivity under the irradiation. In literature, rapid photodegradation of TRI has been attributed to phenoxyl functional group in the literature (Wang et al., 2017).

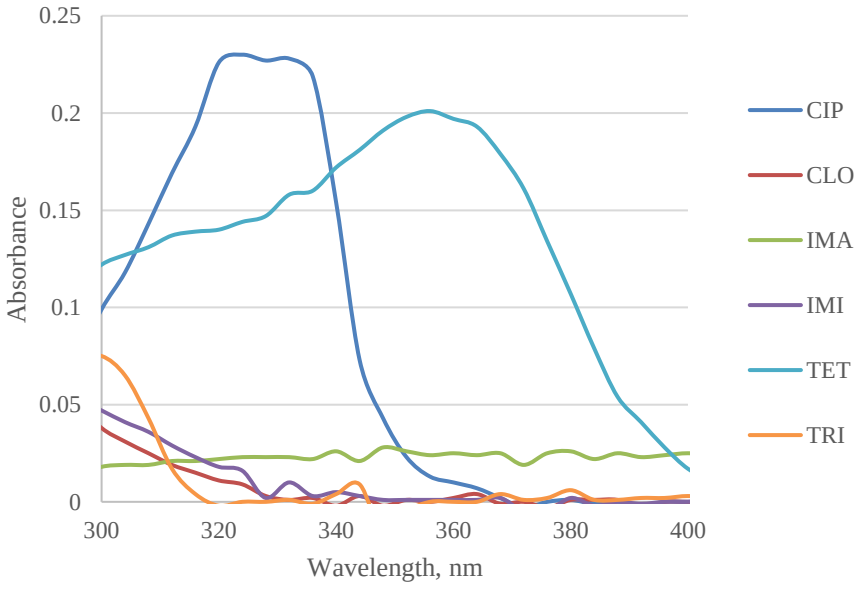

Maximum Absorption Wavelength (nm)	*References*
200-350	(Pereira et al., 2007)
200-460	Keen and Linden, 2013
253.7	(Snowberger et al., 2016)
214.5, 265.5, 290	(Pesticide Properties DataBase)
203, 244, 275	(Pesticide Properties DataBase)
212, 270	(Pesticide Properties DataBase)
200-340	(Ryan, 2009)
200-450	(Werner et al., 2006)
200-340	(Ryan, 2009)
200-700	(Yu et al., 2019)

Figure 4.8. UV-Vis absorption spectra of model ECs in deionized water.

Besides the direct photolysis (Equation 4.7), target contaminants (M) can be degraded by the reaction with reactive species generated from the water components under irradiation (Equations 4.8, 4.9 and 4.10).

$$M + h\nu \rightarrow M^* \quad (4.7)$$

$$CDOM \rightarrow {}^1CDOM^* \rightarrow {}^3CDOM^* \quad (4.8)$$

$$NO_3^- + h\nu \rightarrow NO_3^{-*} \rightarrow NO_2 + O^{\cdot -} + H_2O \rightarrow HO^{\cdot} + OH^- \quad (4.9)$$

$$NO_2^- + h\nu \rightarrow NO_2^{-*} \rightarrow NO + O^{\cdot -} + H_2O \rightarrow HO^{\cdot} + OH^- \quad (4.10)$$

$$M + OH^- \rightarrow transformation\ or\ mineralization\ products \quad (4.11)$$

$$organics, inorganics + reactive\ species \rightarrow products \quad (4.12)$$

The variations in k values in different water samples can be attributed to their compositions. The complex nature of river water can reduce the photodegradation of target ECs. As understood from Table 4.5 and Figure 4.3, the absorbance of the samples at $\lambda < 240$ nm can give the information about the inorganic matter contents. Hence, the inhibition effect of these water constituents on the photolysis rate may be estimated. However, by knowing the direct photolysis pathway of the EC and the constituents of water matrix the photolysis rate cannot be easily estimated in natural water samples due to various reactions occurring at the same time. Although, DOM and NO_3^- are known promoters of photodegradation reactions these constituents together with others (alkalinity, nitrite, etc.) can also scavenge generated reactive species. The photodegradation rates of compounds exhibited relatively lower values in S-5. The discharge of a wastewater treatment plant effluent caused an increase in the concentrations of organic and inorganic compounds at the sampling site of S-5 (Table 4.2 and 4.3). This water sample exhibited high and continuous absorption in the wavelength range of 300-600 nm. Therefore, a shading effect of the river water for the photolysis of spiked ECs would be expected. Besides, a difference in the spectral slope values of S-5, which was considered the dirtiest water matrix, was noticed. Similarly, the spectral properties and chemical composition of S-8 can explain the reason of slightly higher k values of the ECs.

TRI exhibited slower photolysis rate in relatively clean matrix, S-1 although it has light absorption around 300 nm wavelength whereas a higher degradation rate was achieved in S-5 having approximately two-fold higher conductivity (Table 4.6). In literature, the promotion effect of nitrate

ion on the photodegradation of TRI has been reported (Castro et al., 2017). The combined effect of all constituents of water samples my not allow to be seen the positive contribution of the nitrate ion on the photodegradation reaction. Since the compositional changes between the water samples were not drastic k values of TRI could only be differentiated in S-1, which has the lowest nitrate ion concentration. Actually, the degradation rate constants of all ECs at S-8 were higher than those obtained at S-5.

4.2.2. Effects of light intensity on the photodegradation rate of ECs

The intensity of the light is an important factor influencing the lifetime of ECs in aquatic environment. To clarify this effect S-8 spiked with model ECs was exposed to light with intensities ranged from1360 to 810 W m^{-2}. In Table 4.8 and 4.9, photodegradation kinetic rate constants and half-lives of six model ECs are presented, respectively.

Table 4.8. Photodegradation rate constants of six ECs in S-8 exposed to irradiation at different light intensities.

Light Intensity ($W\ m^{-2}$)	**CIP**	**CLO**	**IMA**	**IMI**	**TET**	**TRI**
	k, min^{-1} (R^2)					
1360	0.082 (0.978)	0.021 (0.994)	0.022 (0.995)	0.028 (0.993)	0.328 (0.954)	0.488 (0.974)
1090	0.079 (0.991)	0.014 (0.982)	0.016 (0.986)	0.019 (0.989)	0.344 (0.998)	0.533 (1.000)
865	0.039 (0.990)	0.009 (0.980)	0.010 (0.981)	0.012 (0.975)	0.136 (0.674)	0.308 (0.949)
810	0.022 (0.987)	0.004 (0.987)	0.005 (0.985)	0.006 (0.988)	0.173 (1.000)	0.117 (0.959)

Table 4.9. Half-lives of six ECs in S-8 exposed to irradiation at different light intensities.

Light Intensity ($W\ m^{-2}$)	**CIP**	**CLO**	**IMA**	**IMI**	**TET**	**TRI**
	$t_{1/2}$, min					
1360	8.432	33.485	31.083	24.933	2.113	1.421
1090	8.830	49.511	44.150	36.870	2.013	1.301
865	17.865	77.016	70.729	60.274	5.082	2.248
810	31.796	165.035	144.406	119.508	4.016	5.909

Decreasing the intensity of light diminished the photodegradation rate of all model ECs but the effect was different for each. While this effect was less pronounced for TET which caused remarkable decrease in the concentration during the dark control experiment decreasing the light intensity from 810 $W\ m^{-2}$ to 1360 $W\ m^{-2}$ resulted in more than 4-fold decrease in the rate constants of the ECs exhibited persistent in the darkness.

5. CONCLUSIONS

Ergene River is a significant water source for Thrace region. Although the major part of the Ergene River has “4th class” of water quality currently, it is used for different purposes. It is known that the ecosystem is influenced adversely due to the presence of various contaminants including ECs in the river water and living beings are threatened by detrimental effects of contaminants. Therefore, the photolysis data for ECs obtained in this study can have a contribution for the clarification of one of fate processes in the river water. Such data can also have a critical importance to find a proper way of treatment for river water. Photochemical degradation that can decrease the lifetime of contaminants in the environment, has been investigated for various aquatic pollutants. However, the complicated matrix of urbanized river water can cause the photochemical process to be affected differently. In this study the photolysis fate process of ECs was evaluated by using the river water samples taken from different sites of Ergene River.

In order to study the contribution of agricultural and domestic inputs to the quality of the river water eight different sampling sites ((S-1)-(S-8)) in the study area where the river flows from the source to the point at a distance of 22 km were selected. The detection of seven different ECs including the industrial chemicals even in the site close to the source of the river clearly indicated that uncontrolled discharge and/or atmospheric deposition can cause the contamination of the river water. Two pesticides (diphenilamine and molinate), two corrosion inhibitors (4-methyl-1H-benzotriazole and 5-methyl-1H-benzotriazole), three industrial chemicals (benzosulfonamide, tris(2-butoxyethyl) phosphate and hexa(methoxymethyl)melamine were the quantified ECs. As a result of five hours illumination of (S-1)-(S-8) river water samples under the simulated solar light the concentration of ECs detected did not show any decrease due to their known persistence.

In case of the illumination of eight ((S-1)-(S-8)) river water samples spiked with a mixture of ciprofloxacin, clothianidin, imazamox, imidacloprid, tetracycline, and triclosan almost complete degradation of each them was achieved. The first order model fitted the kinetic data with high correlation for simultaneous degradation of all ECs indicated that the photodegradation rates of tetracycline, triclosan, and ciprofloxacin which are able to absorb light in the wavelength region of lamp emission, were remarkably faster than the other model ECs. Half-lives of all model ECs at 100 ppb initial concentration were less than an hour with 1360 W m^{-2} light intensity. However, the instability of tetracycline and ciprofloxacin should also be considered for their rapid degradation.

The variation of k values in different water matrices indicated that increasing pollution load of the river water resulted in relatively slow reaction. By the flow of the river from S-1 to S-8 sampling site and the discharge of a wastewater treatment plant effluent at S-5 nutrient concentrations together with conductivity increased. PARAFAC modeling of fluorescent spectral data enabled the detection of tryptophan-like and tyrosine-like substances and the fluorescence intensity of protein-like groups between S-1 and S-5 was remarkable. The dissolved iron ion, which is one of the ions having a significant role in photodegradation reactions, has not been detected in any of the river water samples about 2.5-fold difference in concentration of nitrate ion was detected between S-1 and S-8. The k of each EC has the lowest value in S-5. Spectral properties of the river water at different sampling sites exhibited variations and overall results indicated that CDOM of the river in the study area has high molecular weight and terrestrially derived. Although the photochemical reactivity of high molecular weight chromophoric dissolved organic matter together with nitrate could be expected competitive reactions occurred in the water matrix could be accounted as a major reason for slowing down the degradations of ECs. From the results of photolysis experiments conducted in deionized water it can be deduced that direct photolysis was the main photodegradation pathway for ciprofloxacin, tetracycline, and triclosan. The effect of lowering the light intensity from 1360 W m^{-2} to 810 W m^{-2} was almost same on investigated ECs except tetracycline.

REFERENCES

Agüera, A., Bueno, M. J. M., Fernández-Alba, A. R., 2013. New trends in the analytical determination of emerging contaminants and their transformation products in environmental waters. Environmental Science and Pollution Research, 20, 3496-3515.

Agüera López, A., del Mar Gómez Ramos, M., Fernández-Alba, A. R., 2014. Transformation products of pesticides in the environment: Analysis and occurrence. In: Lambropoulou D. A., Nollet L. M. (Eds.), Transformation Products of Emerging Contaminants in the Environment, 385-412, John Wiley and Sons, US.

APHA, AWWA, WEF, 1995. Standard Methods for the Examination of Water and Wastewater, 16th Edition, Washington, D.C., U.S.A.

Archer, E., Petrie, B., Kasprzyk-Hordern, B., Wolfaardt, G. M., 2017. The fate of pharmaceuticals and personal care products (PPCPs), endocrine disrupting contaminants (EDCs), metabolites and illicit drugs in a WWTW and environmental waters. Chemosphere, 174, 437-446.

Arikan, O. A., Rice, C., Codling, E., 2008. Occurrence of antibiotics and hormones in a major agricultural watershed. Desalination, 226, 121-133.

Barbosa, M. O., Moreira, N. F., Ribeiro, A. R., Pereira, M. F., Silva, A. M., 2016. Occurrence and removal of organic micropollutants: An overview of the watch list of EU Decision 2015/495. Water Research, 94, 257-279.

Batchu, S. R., Panditi, V. R., O'Shea, K. E., Gardinali, P. R., 2014. Photodegradation of antibiotics under simulated solar radiation: Implications for their environmental fate. Science of the Total Environment, 470, 299-310.

Batista, A. P. S., Teixeira, A. C. S., Cooper, W. J., Cottrell, B. A., 2016. Correlating the chemical and spectroscopic characteristics of natural organic matter with the photodegradation of sulfamerazine. Water Research, 93, 20-29.

Bobeldijk, I., Stoks, P. G. M., Vissers, J. P. C., Emke, E., Van Leerdam, J. A., Muilwijk, B., Berbee, R., Noij, T. H., 2002. Surface and wastewater quality monitoring: combination of liquid chromatography with (geno) toxicity detection, diode array detection and tandem mass spectrometry for identification of pollutants. Journal of Chromatography A, 970, 167-181.

Bodhipaksha, L. C., Sharpless, C. M., Chin, Y. P., MacKay, A. A., 2017. Role of effluent organic matter in the photochemical degradation of compounds of wastewater origin. Water Research, 110, 170-179.

Bodrato, M., Vione, D., 2014. APEX (Aqueous Photochemistry of Environmentally occurring Xenobiotics): A free software tool to predict the kinetics of photochemical processes in surface waters. Environmental Science: Processes and Impacts, 16, 732-740.

Boreen, A. L., Arnold, W. A., McNeill, K., 2003. Photodegradation of pharmaceuticals in the aquatic environment: A review. Aquatic Sciences, 65, 320-341.

Boreen, A. L., Arnold, W. A., McNeill, K., 2004. Photochemical fate of sulfa drugs in the aquatic environment: Sulfadrugs containing five-membered heterocyclic groups. Environmental Science and Technology, 38, 3933-3940.

Bricaud, A., Morel, A., Prieur, L., 1981. Absorption by dissolved organic matter of the sea (yellow substance) in the UV and visible domains 1. Limnology and Oceanography, 26, 43-53.

Brooks, B. W., Maul, J. D., Belden, J. B., 2008. Emerging Contaminants: Antibiotics in Aquatic and Terrestrial Ecosystems. In: Jorgensen, S. E., Fath, B. D. (Eds.), 210-217, Encyclopedia of Ecology. Elsevier. Oxford. UK.

Bu, Q., Wang, B., Huang, J., Deng, S., Yu, G., 2013. Pharmaceuticals and personal care products in the aquatic environment in China: A review. Journal of Hazardous Materials, 262, 189-211.

Burrows, H. D., Santaballa, J. A., Steenken, S., 2002. Reaction pathways and mechanisms of photodegradation of pesticides. Journal of Photochemistry and Photobiology B: Biology, 67, 71-108.

Calza, P., Vione, D. (Eds.), 2015. Surface Water Photochemistry. Royal Society of Chemistry.

Castro, G., Rodríguez, I., Ramil, M., Cela, R., 2017. Evaluation of nitrate effects in the aqueous photodegradability of selected phenolic pollutants. Chemosphere, 185, 127-136.

Chau, H. T. C., Kadokami, K., Duong, H. T., Kong, L., Nguyen, T. T., Nguyen, T. Q., Ito, Y., 2018. Occurrence of 1153 organic micropollutants in the aquatic environment of Vietnam. Environmental Science and Pollution Research, 25, 7147-7156.

Chung, K. H. Y., Lin, Y. C., Lin, A. Y. C., 2018. The persistence and photostabilizing characteristics of benzotriazole and 5-methyl-1H-benzotriazole reduce the photochemical behavior of common photosensitizers and organic compounds in aqueous environments. Environmental Science and Pollution Research, 25, 5911-5920.

Çevre ve Orman Bakanlığı., 2004. Su Kirliliği Kontrolü Yönetmeliği. Resmi Gazete.

Daghrir, R., Drogui, P., 2013. Tetracycline antibiotics in the environment: A review. Environmental Chemistry Letters, 11, 209-227.

De Haan, H., De Boer, T., 1987. Applicability of light absorbance and fluorescence as measures of concentration and molecular size of dissolved organic carbon in humic Lake Tjeukemeer. Water Research, 21, 731-734.

De Hoogh, C. J., Wagenvoort, A. J., Jonker, F., van Leerdam, J. A., Hogenboom, A. C., 2006. HPLC-DAD and Q-TOF MS techniques identify cause of Daphnia biomonitor alarms in the River Meuse. Environmental Science and Technology, 40, 2678-2685.

De la Cruz, N., Giménez, J., Esplugas, S., Grandjean, D., De Alencastro, L. F., Pulgarin, C., 2012. Degradation of 32 emergent contaminants by UV and neutral photo-fenton in domestic wastewater effluent previously treated by activated sludge. Water Research, 46, 1947-1957.

De Laurentiis, E., Minella, M., Maurino, V., Minero, C., Vione, D., 2014. Effects of climate change on surface-water photochemistry: A review. Environmental Science and Pollution Research, 21, 11770-11780.

Dsikowitzky, L., Schwarzbauer, J., 2015. Hexa (methoxymethyl) melamine: an emerging contaminant in German rivers. Water Environment Research, 87, 461-469.

Durán-Álvarez, J. C., Prado, B., González, D., Sánchez, Y., Jiménez-Cisneros, B., 2015. Environmental fate of naproxen, carbamazepine and triclosan in wastewater, surface water and wastewater irrigated soil—results of laboratory scale experiments. Science of the Total Environment, 538, 350-362.

EU Decision 2015/495, 2015. Establishing a watch list of substances for Union-wide monitoring in the field of water policy pursuant to Directive 2008/105/EC of the European Parliament and of the Council. European Union.

European Water Framework Directive. Updated surface water Watch List adopted by the Commission. https://ec.europa.eu/jrc/en/science-update/updated-surface-water-watch-list-adopted-commission. Date accessed December 2019.

Fairbairn, D. J., Karpuzcu, M. E., Arnold, W. A., Barber, B. L., Kaufenberg, E. F., Koskinen, W. C., Novak, P. J., Rice, P.J., Swackhamer, D. L., 2016. Sources and transport of contaminants of emerging concern: a two-year study of occurrence and spatiotemporal variation in a mixed land use watershed. Science of the Total Environment, 551, 605-613.

Gan, Z., Sun, H., Wang, R., Hu, H., Zhang, P., Ren, X., 2014. Transformation of acesulfame in water under natural sunlight: Joint effect of photolysis and biodegradation. Water Research, 64, 113-122.

Gao, T., Kang, S., Chen, R., Zhang, T., Zhang, T., Han, C., Tripathee, L., Sillanpaa, M., Zhang, Y., 2019. Riverine dissolved organic carbon and its optical properties in a permafrost region of the Upper Heihe River basin in the Northern Tibetan Plateau. Science of the Total Environment, 686, 370-381.

Ge, L., Chen, J., Wei, X., Zhang, S., Qiao, X., Cai, X., Xie, Q., 2010. Aquatic photochemistry of fluoroquinolone antibiotics: Kinetics, pathways, and multivariate effects of main water constituents. Environmental Science and Technology, 44, 2400-2405.

Gonçalves, C., Perez, S., Osorio, V., Petrovic, M., Alpendurada, M. F., Barcelo, D., 2011. Photofate of oseltamivir (Tamiflu) and oseltamivir carboxylate under natural and simulated solar irradiation:

Kinetics, identification of the transformation products, and environmental occurrence. Environmental Science and Technology, 45, 4307-4314.

Gothwal, R., Shashidhar, T., 2015. Antibiotic pollution in the environment: A review. Clean–Soil, Air, Water, 43, 479-489.

Green, S. A., Blough, N. V., 1994. Optical absorption and fluorescence properties of chromophoric dissolved organic matter in natural waters. Limnology and Oceanography, 39, 1903-1916.

Guerard, J. J., Chin, Y. P., Mash, H., Hadad, C. M., 2009. Photochemical fate of sulfadimethoxine in aquaculture waters. Environmental Science and Technology, 43, 8587-8592.

Guillet, G., Knapp, J. L., Merel, S., Cirpka, O. A., Grathwohl, P., Zwiener, C., Schwientek, M., 2019. Fate of wastewater contaminants in rivers: Using conservative-tracer based transfer functions to assess reactive transport. Science of the Total Environment, 656, 1250-1260.

Han, X., Li, Y., Li, D., Liu, C., 2017. Role of free radicals/reactive oxygen species in MeHg photodegradation: Importance of utilizing appropriate scavengers. Environmental Science and Technology, 51, 3784-3793.

He, J., Li, J., Ma, L., Wu, N., Zhang, Y., Niu, Z., 2019. Large-scale distribution of organophosphate esters (flame retardants and plasticizers) in soil from residential area across China: Implications for current level. Science of The Total Environment, 697, 133997.

Helms, J. R., Stubbins, A., Ritchie, J. D., Minor, E. C., Kieber, D. J., Mopper, K., 2008. Absorption spectral slopes and slope ratios as indicators of molecular weight, source, and photobleaching of chromophoric dissolved organic matter. Limnology and Oceanography, 53, 955-969.

Herrero, P., Borrull, F., Pocurull, E., Marcé, R. M., 2013. Efficient tandem solid-phase extraction and liquid chromatography-triple quadrupole mass spectrometry method to determine polar benzotriazole, benzothiazole and benzenesulfonamide contaminants in environmental water samples. Journal of Chromatography A, 1309, 22-32.

Herrero, P., Borrull, F., Pocurull, E., Marcé, R. M., 2014. An overview of analytical methods and occurrence of benzotriazoles, benzothiazoles and benzenesulfonamides in the environment. TrAC Trends in Analytical Chemistry, 62, 46-55.

Huntscha, S., Hofstetter, T. B., Schymanski, E. L., Spahr, S., Hollender, J., 2014. Biotransformation of benzotriazoles: Insights from transformation product identification and compound-specific isotope analysis. Environmental Science and Technology, 48, 4435-4443.

Ingle, M., D'souza, M. C., 1989. Physiology and control of superficial scald of apples: A review. HortScience, 24, 28-31.

Jim, T. Y., Bouwer, E. J., Coelhan, M., 2006. Occurrence and biodegradability studies of selected pharmaceuticals and personal care products in sewage effluent. Agricultural Water Management, 86, 72-80.

Jover, E., Matamoros, V., Bayona, J. M., 2009. Characterization of benzothiazoles, benzotriazoles and benzosulfonamides in aqueous matrixes by solid-phase extraction followed by comprehensive two-dimensional gas chromatography coupled to time-of-flight mass spectrometry. Journal of Chromatography A, 1216, 4013-4019.

Jurado, A., Vàzquez-Suñé, E., Carrera, J., de Alda, M. L., Pujades, E., Barceló, D., 2012. Emerging organic contaminants in groundwater in Spain: A review of sources, recent occurrence and fate in a European context. Science of the Total Environment, 440, 82-94.

Keen, O. S., Linden, K. G., 2013. Degradation of antibiotic activity during UV/H_2O_2 advanced oxidation and photolysis in wastewater effluent. Environmental Science and Technology, 47, 13020-13030.

Kelly, M. M., Arnold, W. A., 2012. Direct and indirect photolysis of the phytoestrogens genistein and daidzein. Environmental Science and Technology, 46, 5396-5403.

Kirk, J. T., 1994. Light and Photosynthesis in Aquatic Ecosystems. Cambridge University Press, UK.

Kiss, A., Fries, E., 2009. Occurrence of benzotriazoles in the rivers Main, Hengstbach, and Hegbach (Germany). Environmental Science and Pollution Research, 16, 702-710.

Klementova, S., 2018. Photochemical Degradation of Organic Xenobiotics in Natural Waters. In: Saha, S., & Mondal, S. (Eds.), Photochemistry and Photophysics: Fundamentals to Applications, 67-88, IntechOpen, London, UK.

Konstantinou, I. K., Zarkadis, A. K., Albanis, T. A., 2001. Photodegradation of selected herbicides in various natural waters and soils under environmental conditions. Journal of Environmental Quality, 30, 121-130.

K'oreje, K. O., Kandie, F. J., Vergeynst, L., Abira, M. A., Van Langenhove, H., Okoth, M., Demeestere, K., 2018. Occurrence, fate and removal of pharmaceuticals, personal care products and pesticides in wastewater stabilization ponds and receiving rivers in the Nzoia Basin, Kenya. Science of the Total Environment, 637, 336-348.

Lei, X., Pan, J., Devlin, A. T., 2019. Characteristics of absorption spectra of chromophoric dissolved organic matter in the Pearl River Estuary in spring. Remote Sensing, 11, 1533.

Leifer, A., 1988. The Kinetics of Environmental Aquatic Photochemistry: Theory and Practice. American Chemical Society, Washington, US.

Li, W. X., Chen, M., Chen, W. T., Qiao, C. K., Li, M. H., Han, L. J., 2012. Determination of mepiquat chloride in cotton crops and soil and its dissipation rates. Ecotoxicology and Environmental Safety, 85, 137-143.

Li, P., Hur, J., 2017. Utilization of UV-Vis spectroscopy and related data analyses for dissolved organic matter (DOM) studies: A review. Critical Reviews in Environmental Science and Technology, 47, 131-154.

Lin, A. Y. C., Reinhard, M., 2005. Photodegradation of common environmental pharmaceuticals and estrogens in river water. Environmental Toxicology and Chemistry: An International Journal, 24, 1303-1309.

Liu, X., Ji, K., Choi, K. 2012. Endocrine disruption potentials of organophosphate flame retardants and related mechanisms in H295R and MVLN cell lines and in zebrafish. Aquatic Toxicology, 114, 173-181.

Luo, Y., Guo, W., Ngo, H. H., Nghiem, L. D., Hai, F. I., Zhang, J., Liang, S., Wang, X. C., 2014. A review on the occurrence of micropollutants in the aquatic environment and their fate and removal during wastewater treatment. Science of the Total Environment, 473, 619-641.

Maier, D., Blaha, L., Giesy, J. P., Henneberg, A., Köhler, H. R., Kuch, B., Osteraurer, R., Peschke, K., Richter, D., Scheurer, M., Triebskorn, R., 2015. Biological plausibility as a tool to associate analytical data for micropollutants and effect potentials in wastewater, surface water, and sediments with effects in fishes. Water Research, 72, 127-144.

Manamsa, K., Lapworth, D. J., Stuart, M. E., 2016. Temporal variability of micro-organic contaminants in lowland chalk catchments: New insights into contaminant sources and hydrological processes. Science of the Total Environment, 568, 566-577.

Mangalgiri, K. P., Blaney, L., 2017. Elucidating the stimulatory and inhibitory effects of dissolved organic matter from poultry litter on photodegradation of antibiotics. Environmental Science and Technology, 51, 12310-12320.

Meffe, R., de Bustamante, I., 2014. Emerging organic contaminants in surface water and groundwater: A first overview of the situation in Italy. Science of the Total Environment, 481, 280-295.

Michael, I., Vasquez, M. I., Hapeshi, E., Haddad, T., Baginska, E., Kümmerer, K., Fatta-Kassinos, D., 2014. Metabolites and transformation products of pharmaceuticals in the aquatic environment as contaminants of emerging concern. Transformation Products of Emerging Contaminants in the Environment, 413-457.

Moldovan, Z., Marincas, O., Povar, I., Lupascu, T., Longree, P., Rota, J. S., Singer, H., Alder, A. C., 2018. Environmental exposure of anthropogenic micropollutants in the Prut River at the Romanian-Moldavian border: A snapshot in the lower Danube river basin. Environmental Science and Pollution Research, 25, 31040-31050.

Moschet, C., Vermeirssen, E. L., Singer, H., Stamm, C., Hollender, J., 2015. Evaluation of in-situ calibration of Chemcatcher passive samplers for 322 micropollutants in agricultural and urban affected rivers. Water Research, 71, 306-317.

Mulligan, R. A., Redman, Z. C., Keener, M. R., Ball, D. B., Tjeerdema, R. S., 2016. Photodegradation of clothianidin under simulated California rice field conditions. Pest Management Science, 72, 1322-1327.

Nelson, N. B., Siegel, D. A., 2013. The global distribution and dynamics of chromophoric dissolved organic matter. Annual Review of Marine Science, 5, 447-476.

Noutsopoulos, C., Koumaki, E., Sarantopoulos, V., Mamais, D., 2019. Analytical and mathematical assessment of emerging pollutants fate in a river system. Journal of Hazardous Materials, 364, 48-58.

Osburn, C. L., Handsel, L. T., Peierls, B. L., Paerl, H. W., 2016. Predicting sources of dissolved organic nitrogen to an estuary from an agro-urban coastal watershed. Environmental Science and Technology, 50, 8473-8484.

Orman ve Su İşleri Bakanlığı., 2016. Yerüstü Su Kalitesi Yönetmeliğinde Değişiklik Yapılmasına Dair Yönetmelik. Resmi Gazete.

Pal, A., Gin, K. Y. H., Lin, A. Y. C., Reinhard, M., 2010. Impacts of emerging organic contaminants on freshwater resources: review of recent occurrences, sources, fate and effects. Science of the Total Environment, 408, 6062-6069.

Pereira, V. J., Weinberg, H. S., Linden, K. G., Singer, P. C., 2007. UV degradation kinetics and modeling of pharmaceutical compounds in laboratory grade and surface water via direct and indirect photolysis at 254 nm. Environmental Science and Technology, 1682-1688.

Petrie, B., Barden, R., Kasprzyk-Hordern, B., 2015. A review on emerging contaminants in wastewaters and the environment: Current knowledge, understudied areas and recommendations for future monitoring. Water Research, 72, 3-27.

Pesticide Properties DataBase. https://sitem.herts.ac.uk/aeru/ppdb/en/index.htm. Date accessed December 2019.

Potter, B. B., Wimsatt, J. C., 2005. Method 415.3. Determination of total organic carbon and specific UV absorbance at 254 nm in source water and drinking water. US Environmental Protection Agency, Cincinnati, US.

Quesada, H. B., Baptista, A. T. A., Cusioli, L. F., Seibert, D., de Oliveira Bezerra, C., Bergamasco, R., 2019. Surface water pollution by pharmaceuticals and an alternative of removal by low-cost adsorbents: A review. Chemosphere, 222, 766-780.

Remucal, C. K., 2014. The role of indirect photochemical degradation in the environmental fate of pesticides: A review. Environmental Science: Processes and Impacts, 16, 628-653.

Robles-Molina, J., Gilbert-López, B., García-Reyes, J. F., Molina-Díaz, A., 2014. Monitoring of selected priority and emerging contaminants in the Guadalquivir River and other related surface waters in the province of Jaén, South East Spain. Science of the Total Environment, 479, 247-257.

Rosenfeld, P. E., Feng, L., 2011. Risks of Hazardous Wastes. William Andrew. UK.

Ruhala, S. S., Zarnetske, J. P., 2017. Using in-situ optical sensors to study dissolved organic carbon dynamics of streams and watersheds: A review. Science of the Total Environment, 575, 713-723.

Ryan, C. C., 2009. Photolysis and Digestion as Polishing Steps for the Removal of Antibiotics from Municipal Wastewater Treatment Plant Effluent and Biosolids, M.Sc. Thesis, University of Minnesota, US.

Ryan, C. C., Tan, D. T., Arnold, W. A., 2011. Direct and indirect photolysis of sulfamethoxazole and trimethoprim in wastewater treatment plant effluent. Water Research, 45, 1280-1286.

Santoke, H., Cooper, W. J., 2017. Environmental photochemical fate of selected pharmaceutical compounds in natural and reconstituted Suwannee River water: Role of reactive species in indirect photolysis. Science of the Total Environment, 580, 626-631.

Schwarzbauer, J., Ricking, M., 2010. Non-target screening analysis of river water as compound-related base for monitoring measures. Environmental Science and Pollution Research, 17, 934-947.

Schwarzenbach, R. P., Gschwend, P. M., Imboden D. M., 2017. Environmental Organic Chemistry. John Wiley and Sons, US.

Shao, T., Song, K., Jacinthe, P. A., Du, J., Zhao, Y., Ding, Z., Guan, Y., Bai, Z., 2016. Characteristics and sources analysis of riverine chromophoric dissolved organic matter in Liaohe River, China. Water Science and Technology, 74, 2843-2859.

Silva, E., Daam, M. A., Cerejeira, M. J., 2015. Aquatic risk assessment of priority and other river basin specific pesticides in surface waters of Mediterranean river basins. Chemosphere, 135, 394-402.

Śliwka-Kaszyńska, M., Jakimska-Nagórska, A., Wasik, A., Kot-Wasik, A., 2019. Phototransformation of three selected pharmaceuticals, naproxen, 17α-Ethinylestradiol and tetracycline in water: Identification of photoproducts and transformation pathways. Microchemical Journal, 148, 673-683.

Snowberger, S., Adejumo, H., He, K., Mangalgiri, K. P., Hopanna, M., Soares, A. D., Blaney, L. 2016. Direct photolysis of fluoroquinolone antibiotics at 253.7 nm: Specific reaction kinetics and formation of equally potent fluoroquinolone antibiotics. Environmental Science and Technology, 50, 9533-9542.

Sousa, J. C., Ribeiro, A. R., Barbosa, M. O., Pereira, M. F. R., Silva, A. M., 2018. A review on environmental monitoring of water organic pollutants identified by EU guidelines. Journal of Hazardous Materials, 344, 146-162.

Spencer, R. G., Baker, A., Ahad, J. M., Cowie, G. L., Ganeshram, R., Upstill-Goddard, R. C., Uher, G., 2007. Discriminatory classification of natural and anthropogenic waters in two UK estuaries. Science of the Total Environment, 373, 305-323.

Stasinakis, A. S., Gatidou, G., 2010. Micropollutants and Aquatic Environment. In: Virkutye J., Varma R. S., Jegatheesan V. (Eds.), Treatment of Micropollutants in Water and Wastewater, 1-35, London, IWA Publishing, UK.

Stedmon, C. A., Bro, R., 2008. Characterizing dissolved organic matter fluorescence with parallel factor analysis: a tutorial. Limnology and Oceanography: Methods, 6, 572-579.

Stedmon, C. A., Bro, R., 2009, DOMFluor Toolbox, version 1.7.

Stedmon, C. A., Markager, S., Kaas, H., 2000. Optical properties and signatures of chromophoric dissolved organic matter (CDOM) in Danish coastal waters. Estuarine, Coastal and Shelf Science, 51, 267-278.

Stedmon, C. A., Nelson, N. B., 2015. The Optical Properties of DOM in the Ocean. In: Hansell, D. A., Carlson, C. A. (Eds.), Biogeochemistry of Marine Dissolved Organic Matter, 481-508, Academic Press, New York, US.

Szymańska, U., Wiergowski, M., Sołtyszewski, I., Kuzemko, J., Wiergowska, G., Woźniak, M. K. 2019. Presence of antibiotics in the aquatic environment in Europe and their analytical monitoring: Recent trends and perspectives. Microchemical Journal, 147, 729-740.

Ter Halle, A., Richard, C., 2006. Simulated solar light irradiation of mesotrione in natural waters. Environmental Science and Technology, 40, 3842-3847.

Tezel, U., Ayvaz, M. T., Balcıoğlu, I., Gölge, M., Göktaş, R. K., Hanedar, A., Kentel, E., Sandıkkaya, M. T., Tezel, B. K., 2019. Development of a geographical information systems based decision-making tool for water quality management of Ergene watershed using pollutant fingerprint. No:115Y064. The Scientific and Technological Research Council of Turkey.

The MathWorks, 2018, MATLAB R2018a Curve Fitting Toolbox. Natick, MA, US.

Thuyet, D. Q., Watanabe, H., Yamazaki, K., Takagi, K., 2011. Photodegradation of imidacloprid and fipronil in rice–paddy water. Bulletin of Environmental Contamination and Toxicology, 86, 548-553.

Todey, S. A., Fallon, A. M., Arnold, W. A., 2018. Neonicotinoid insecticide hydrolysis and photolysis: Rates and residual toxicity. Environmental Toxicology and Chemistry, 37, 2797-2809.

Tsaboula, A., Papadakis, E. N., Vryzas, Z., Kotopoulou, A., Kintzikoglou, K., Papadopoulou-Mourkidou, E., 2016. Environmental and human risk hierarchy of pesticides: A prioritization method, based on monitoring, hazard assessment and environmental fate. Environment International, 91, 78-93.

Vione, D., Fabbri, D., Minella, M., Canonica, S., 2018. Effects of the antioxidant moieties of dissolved organic matter on triplet-sensitized phototransformation processes: Implications for the photochemical modeling of sulfadiazine. Water Research, 128, 38-48.

Vione, D., Chiron, S., 2014. Phototransformation Processes of Emerging Contaminants in Surface Water. In: Lambropoulou, D. A., Nollet, L. M. L. (Eds.), Transformation Products of Emerging Contaminants in the Environment, 87-122. John Wiley and Sons, US.

Wang, Y., Roddick, F. A., Fan, L., 2017. Direct and indirect photolysis of seven micropollutants in secondary effluent from a wastewater lagoon. Chemosphere, 185, 297-308.

Wei, C. J., Li, X. Y., Xie, Y. F., Wang, X. M., 2019. Direct photo transformation of tetracycline and sulfanomide group antibiotics in surface water: Kinetics, toxicity and site modeling. Science of the Total Environment, 686, 1-9.

Weidauer, C., Davis, C., Raeke, J., Seiwert, B., Reemtsma, T., 2016. Sunlight photolysis of benzotriazoles–Identification of transformation products and pathways. Chemosphere, 154, 416-424.

Werner, J. J., Arnold, W. A., McNeill, K., 2006. Water hardness as a photochemical parameter: tetracycline photolysis as a function of calcium concentration, magnesium concentration, and pH. Environmental Science and Technology, 40, 7236-7241.

Wilkinson, J., Hooda, P. S., Barker, J., Barton, S., Swinden, J., 2017. Occurrence, fate and transformation of emerging contaminants in water: An overarching review of the field. Environmental Pollution, 231, 954-970.

World Health Organization Website. https://www.who.int/mediacentre/news/releases/2018/antibiotic-resistance-found/en/. Date accessed December 2019.

Wozniak, B., Dera, J., 2007. Light Absorption in Sea Water, Springer. New York, US.

Xiao, Y. H., Sara-Aho, T., Hartikainen, H., Vähätalo, A. V., 2013. Contribution of ferric iron to light absorption by chromophoric dissolved organic matter. Limnology and Oceanography, 58, 653-662.

Xie, H., Wang, X., Chen, J., Li, X., Jia, G., Zou, Y., Zhang, Y., Cui, Y., 2019. Occurrence, distribution and ecological risks of antibiotics and pesticides in coastal waters around Liaodong Peninsula, China. Science of The Total Environment, 656, 946-951.

Yang, L., Han, D. H., Lee, B. M., Hur, J., 2015. Characterizing treated wastewaters of different industries using clustered fluorescence EEM–PARAFAC and FT-IR spectroscopy: Implications for downstream impact and source identification. Chemosphere, 127, 222-228.

Yu, H. W., Park, M., Wu, S., Lopez, I. J., Ji, W., Scheideler, J., Snyder, S. A., 2019. Strategies for selecting indicator compounds to assess attenuation of emerging contaminants during UV advanced oxidation processes. Water Research, 166, 115030.

Zhou, C., Chen, J., Xie, Q., Wei, X., Zhang, Y. N., Fu, Z., 2015. Photolysis of three antiviral drugs acyclovir, zidovudine and lamivudine in surface freshwater and seawater. Chemosphere, 138, 792-797.

Zhou, C., Chen, J., Xie, H., Zhang, Y. N., Li, Y., Wang, Y., Xie, Q. Zhang, S. 2018. Modeling photodegradation kinetics of organic micropollutants in water bodies: A case of the Yellow River estuary. Journal of Hazardous Materials, 349, 60-67.

Zhou, Y., Martin, P., Müller, M., 2019. Composition and cycling of dissolved organic matter from tropical peatlands of coastal Sarawak, Borneo, revealed by fluorescence spectroscopy and parallel factor analysis. Biogeosciences, 16, 2733-2749.

APPENDIX A: CHEMICAL PROPERTIES OF NON-TARGET SCREENING CONTAMINANTS

Chemical Name	CAS number	Molecular formula	Molecular structure	Solubility (mg/L)	LogP
1,2,3-Benzotriazole	95-14-7	$C_6H_5N_3$	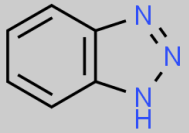	19800	1.44
3-Chloroaniline	108-42-9	C_6H_6ClN	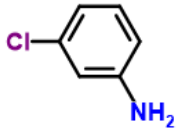	5400	1.88
4,4'-Dichlorobenzophenone	90-98-2	$C_{13}H_8Cl_2O$	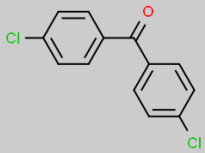	0.83	2.154
4-Methyl-1H-benzotriazole	29878-31-7	$C_7H_7N_3$	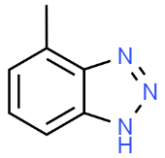	1924.9	0.763
5,6-Dimethyl-1H-benzotriazole monohydrate	4184-79-6	$C_8H_{11}N_3O$	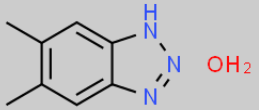	914.20	0.899
5-Methyl-1H-benzotriazole (5-Tolytriazole)	136-85-6	$C_7H_7N_3$	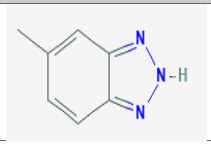	3069	0.974

Acetaminophen (Paracetamol)	103-90-2	$C_8H_9NO_2$	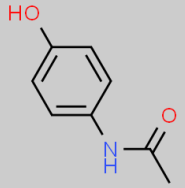	14000	0.46
Acetamiprid	135410-20-7	$C_{10}H_{11}ClN_4$	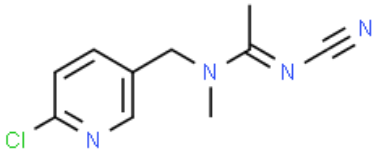	4200	0.8
Aclonifen	74070-46-5	$C_{12}H_9ClN_2O_3$	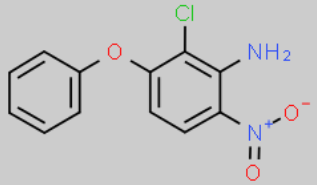	2.5	4.04
Amoxicillin	26787-78-0	$C_{16}H_{19}N_3O_5S$	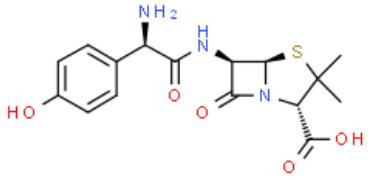	3430	0.87
Atrazine	1912-24-9	$C_8H_{14}ClN_5$	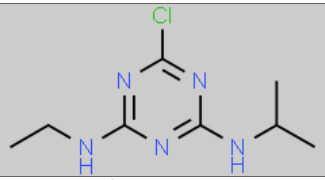	34.70	2.61
Azithromycin	83905-01-5	$C_{38}H_{72}N_2O_{12}$	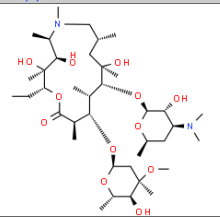	7.09	4.02

Azoxystrobin	131860-33-8	$C_{22}H_{17}N_3O_5$	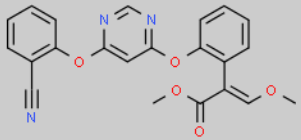	6.00	2.50
Benzenesulfonamide	98-10-2	$C_6H_7NO_2S$	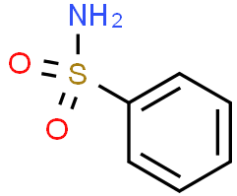	4300	0.31
Benzylamine	100-46-9	C_7H_9N	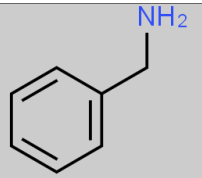	1.0×10^6	1.09
Benzyltrimethylammonium	14800-24-9	$C_{10}H_{16}N$	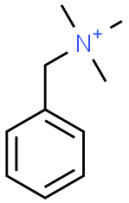	1000000	-0.47
Boisvelone / Iso-Esuper	54464-57-2	$C_{16}H_{26}O$	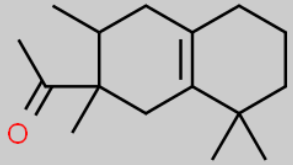	1.08	3.919
Cadusafos	95465-99-9	$C_{10}H_{23}O_2PS_2$	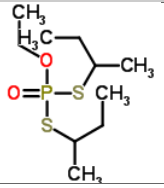	248	3.90

Carbazole	86-74-8	$C_{12}H_9N$	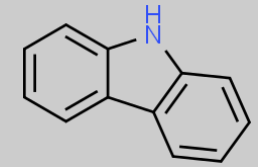	1.8	3.72
Carbendazim	10605-21-7	$C_9H_9N_3O_2$	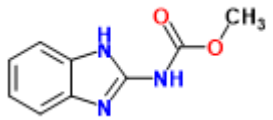	29	1.52
Ciprofloxacin	85721-33-1	$C_{17}H_{18}FN_3O_3$	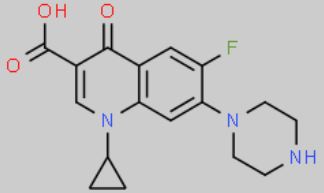	30000	0.28
Clarithromycin	81103-11-9	$C_{38}H_{69}NO_{13}$	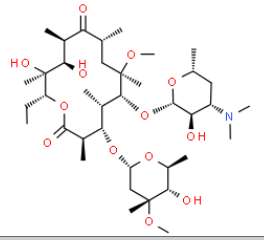	0.34	3.16
Di(2- ethylhexyl)phthalate (DEHP)	117-81-7	$C_{24}H_{38}O_4$	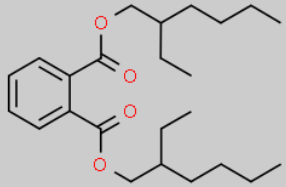	0.27	7.60
Diphenylamine	122-39-4	$C_{12}H_{11}N$	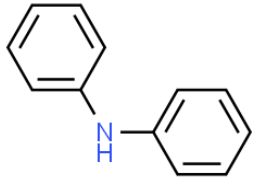	53.00	3.50

Diuron	330-54-1	$C_9H_{10}Cl_2N_2O$	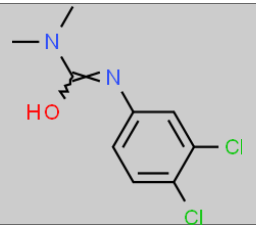	42.00	2.68
Drometrizole	2440-22-4	$C_{13}H_{11}N_3O$	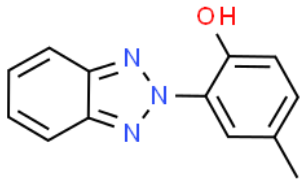	25.59	4.31
Epoxiconazole	106325-08-0	$C_{17}H_{13}ClFN_3O$	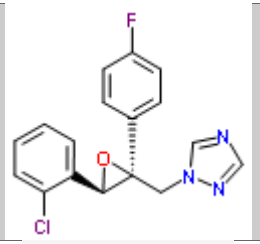	6.63	3.44
Ethylhexylmethoxycinnamate	5466-77-3	$C_{18}H_{25}O_3^-$	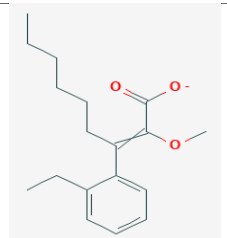	0.15	5.8
Galaxolide	1222-05-5	$C_{18}H_{26}O$	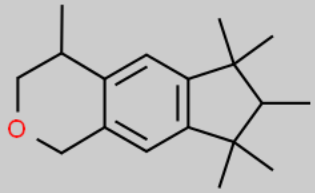	1.75	5.9

Hexa(methoxymethyl)melamine	68002-20-0	$C_{15}H_{30}N_6O_6$	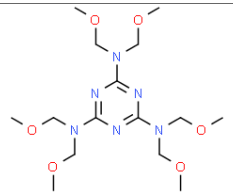	149.30	3.07
Mepiquat chloride	24307.26.4	$C_7H_{16}ClN$	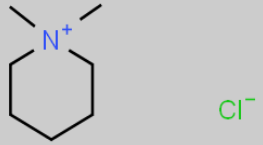	$5.0*10^5$	-2.82
Metolachlor	51218-45-2	$C_{15}H_{12}ClNO_2$	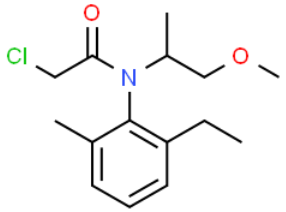	530	3.13
Microcystin-RR	111755-37-4	$C_{49}H_{75}N_{13}O_{12}$	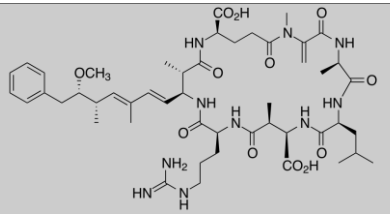	-	-3.96
Molinate	2212.67.1	$C_9H_{17}NOS$	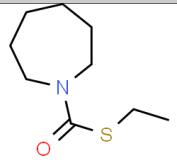	970	3.21
Myclobutanil	88671-89-0	$C_{15}H_{17}ClN_4$	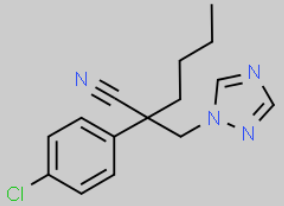	142	2.94

N-Benzyldimethylamine	103-83-3	$C_9H_{13}N$	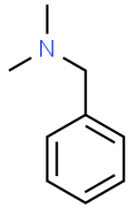	1.2×10^4	1.98
Norfloxacin	70458-96-7	$C_{16}H_{18}FN_3O_3$	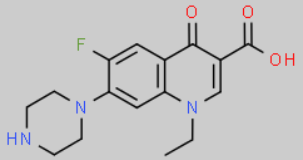	1.78×10^5	-1.03
Ofloxacin	82419-36-1	$C_{18}H_{20}FN_3O_4$	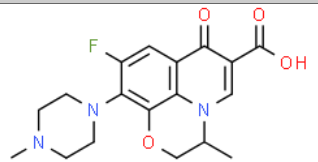	2.83×10^4	-0.39
Prochloraz	67747-09-5	$C_{15}H_{16}Cl_3N_3O_2$	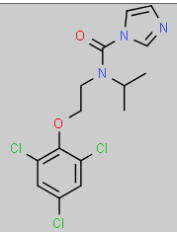	34	4.1
Prometryn	7287-19-6	$C_{10}H_{19}N_5S$	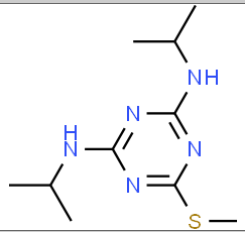	33	3.51
Prothioconazole	178928-70-6	$C_{14}H_{15}Cl_2N_3OS$	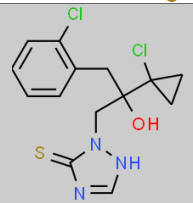	5.53	1.647

Quinalphos	13593-03-8	$C_{12}H_{15}N_2O_3PS$	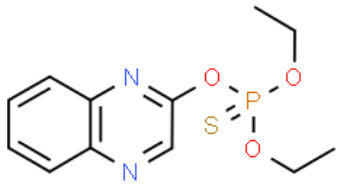	22	4.44
Sulfamethoxazole	723-46-6	$C_{10}H_{11}N_3O_3S$	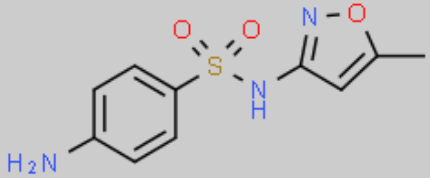	610	0.89
Tebuconazole	107534-96-3	$C_{16}H_{22}ClN_3O$	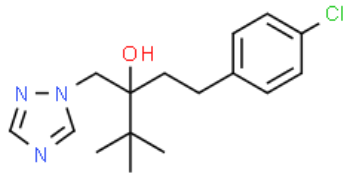	36	3.70
Terbutryn	886-50-0	$C_{10}H_{19}N_5O$	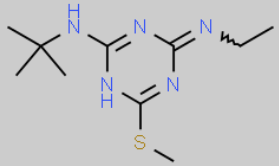	25	3.74
Tetraacetylethylenediamine	10543-57-4	$C_{10}H_{19}N_5S$	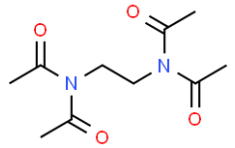	200	0.394
Tetracycline	60-54-8	$C_{22}H_{24}N_2O_8$	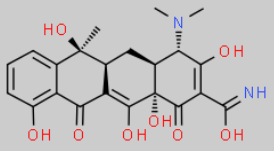	231	-1.30
Thiacloprid	111988-49-9	$C_{10}H_9N_5S$	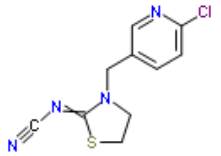	185	1.26

Triphenylphosphineoxide	791-28-6	$C_{18}H_{15}OP$	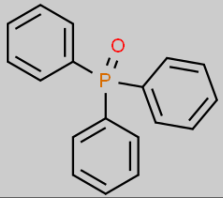	62.8	2.83
Tris(2-butoxyethyl) phosphate	78-51-3	$C_{18}H_{39}O_7P$	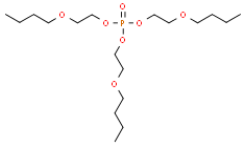	1100	3.75

APPENDIX B: CALIBRATION GRAPHS AND CHROMATOGRAMS OF TARGET SCREENING CONTAMINANTS

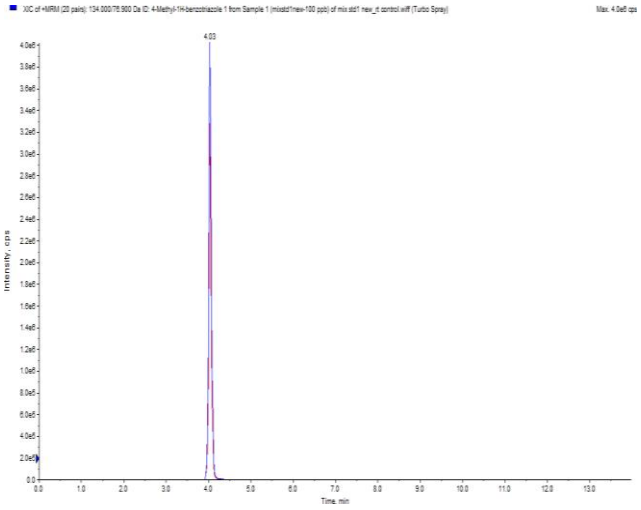

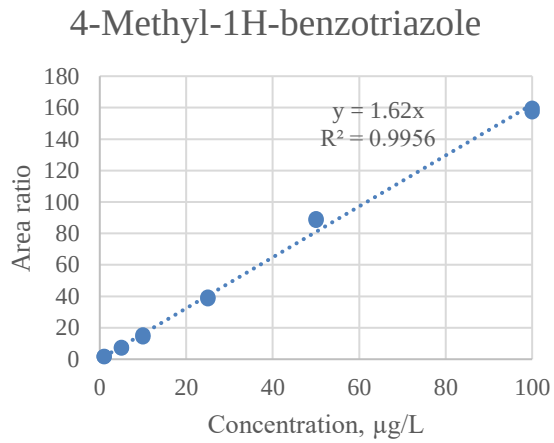

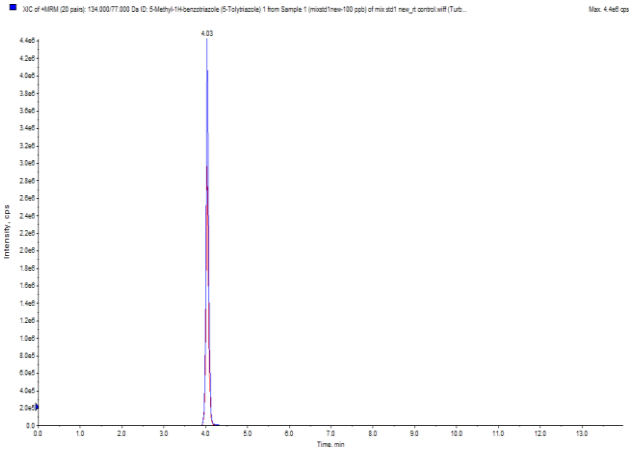

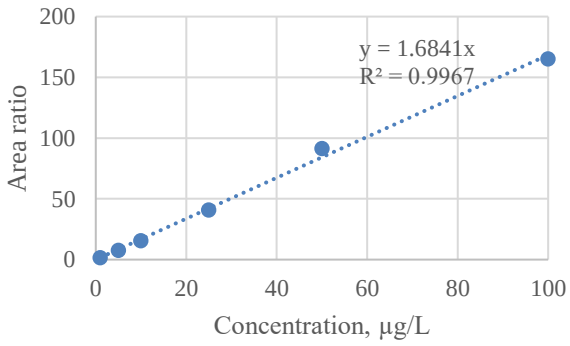

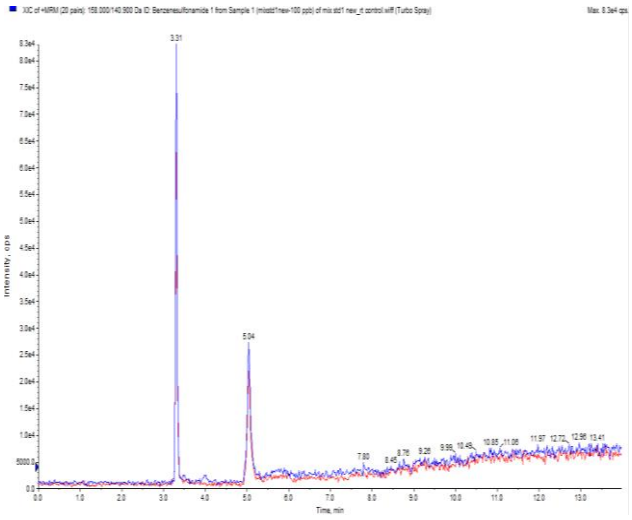

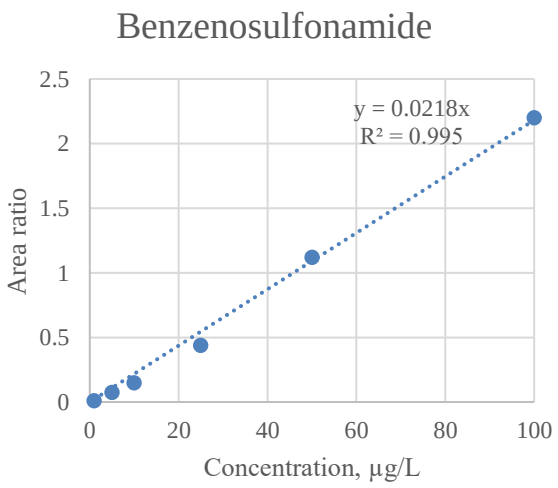

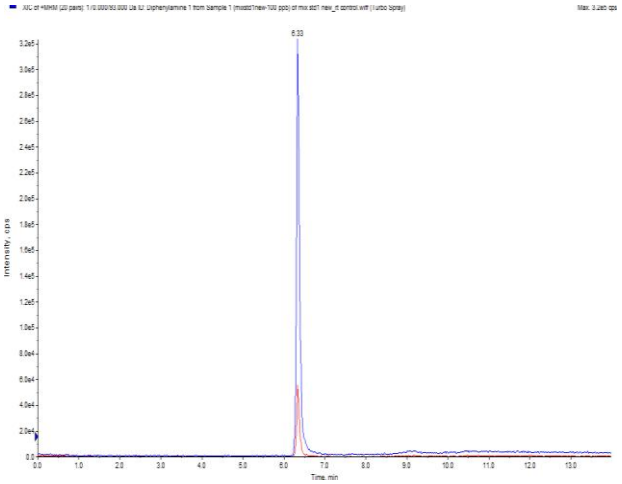

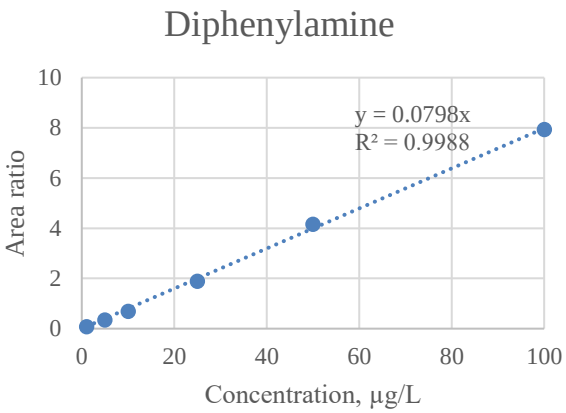
Diphenylamine
y = 0.0798x
R² = 0.9988
Area ratio
Concentration, µg/L

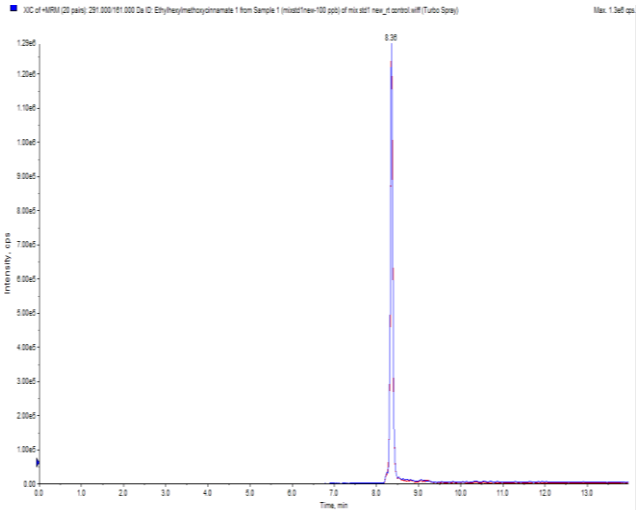

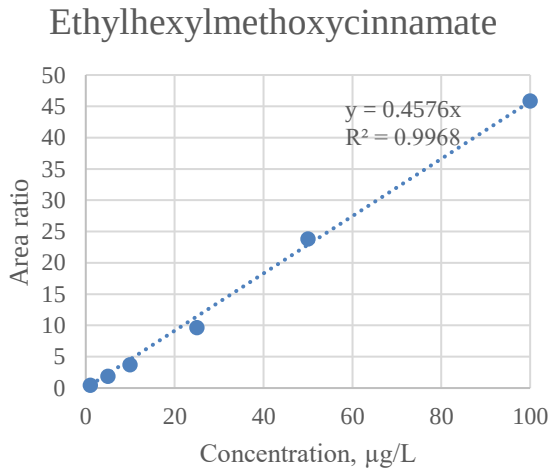
Ethylhexylmethoxycinnamate
y = 0.4576x
R² = 0.9968
Area ratio
Concentration, µg/L

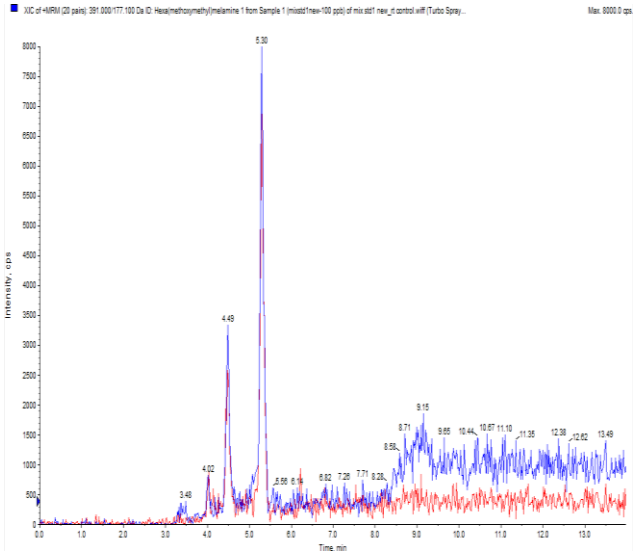

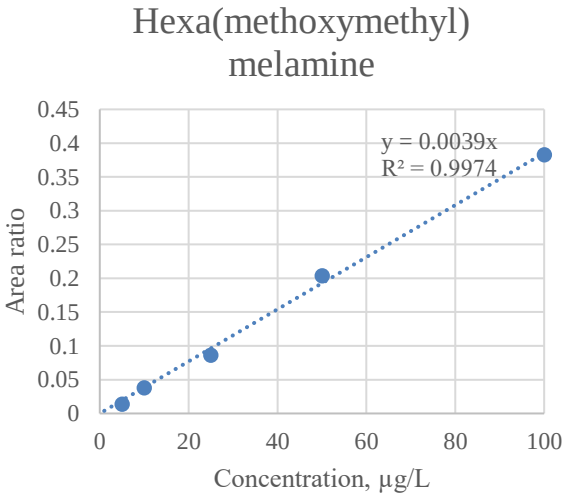
Hexa(methoxymethyl)
melamine
y = 0.0039x
R² = 0.9974
Area ratio
Concentration, µg/L

APPENDIX C: CALIBRATION GRAPHS AND CHROMATOGRAMS OF MODEL CONTAMINANTS

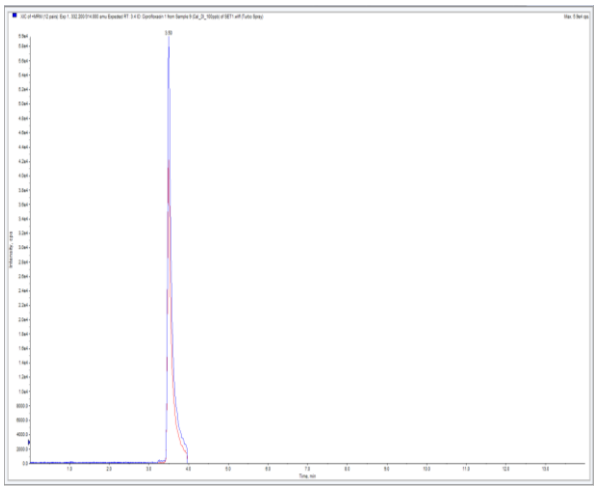

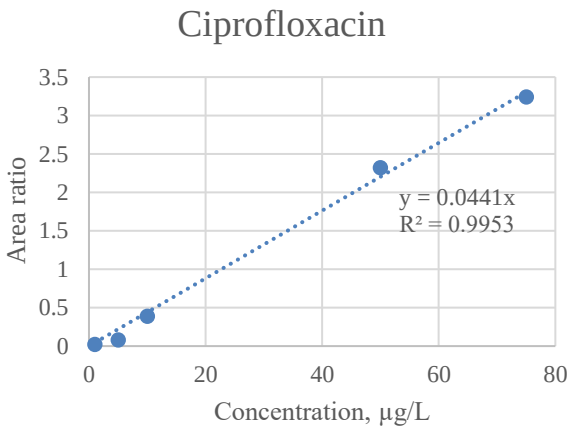

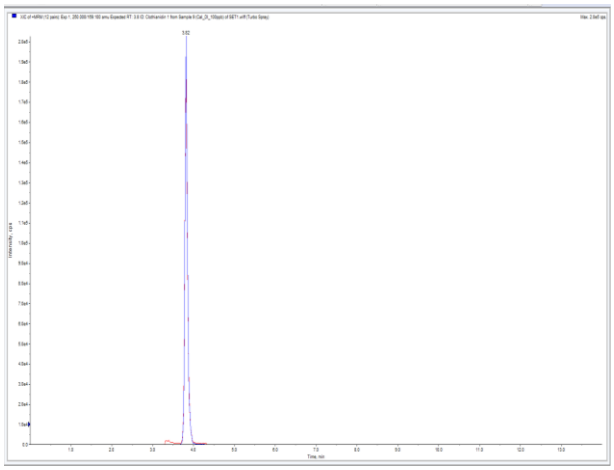

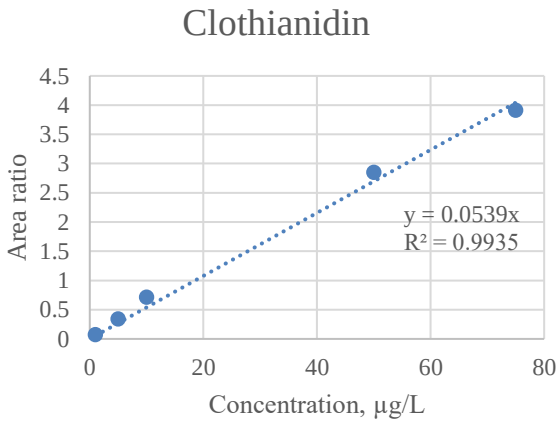

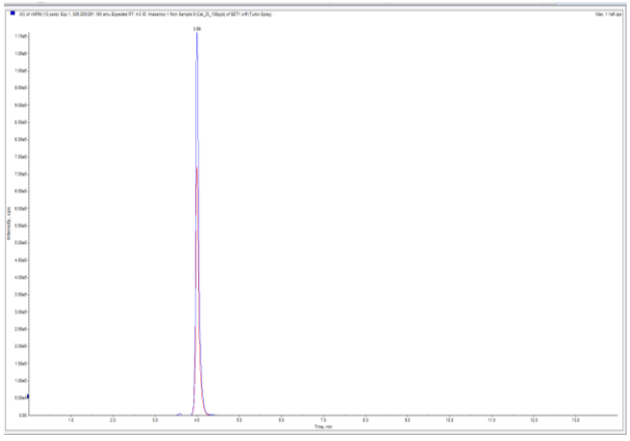

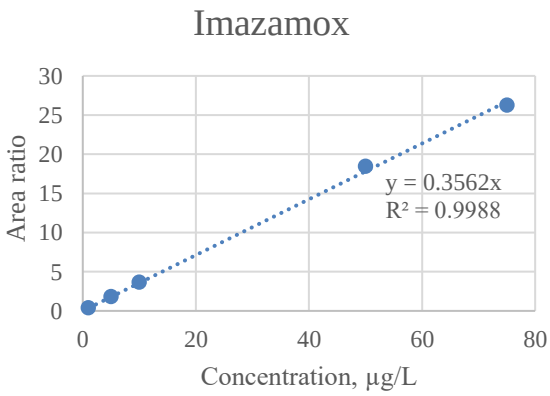

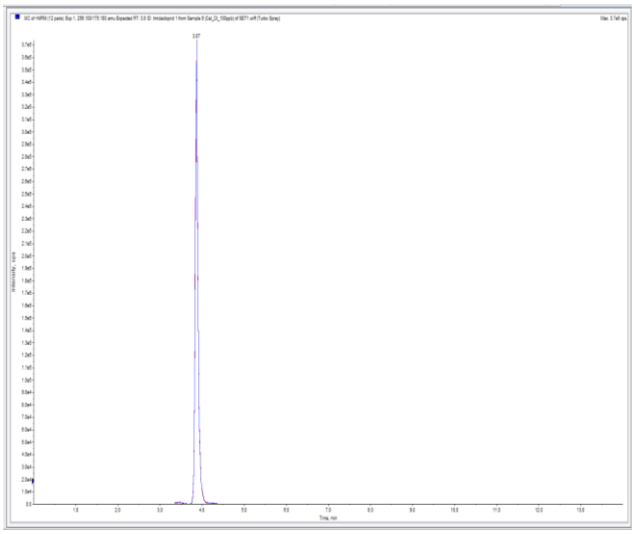

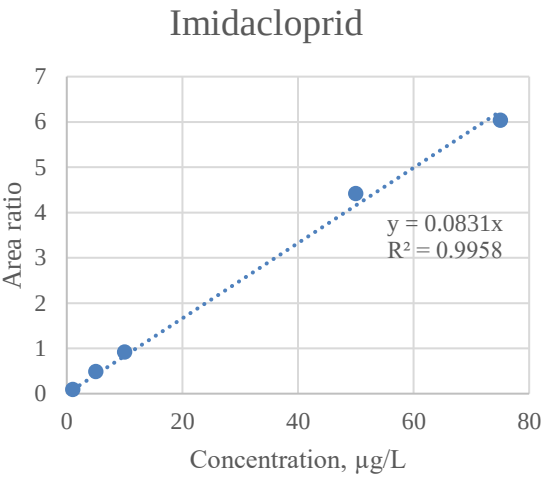
Imidacloprid
Area ratio
Concentration, µg/L
y = 0.0831x
R² = 0.9958
0
1
2
3
4
5
6
7
0
20
40
60
80

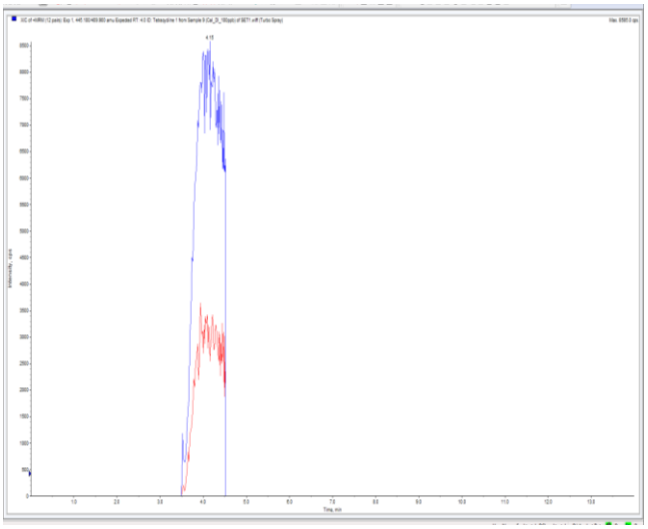

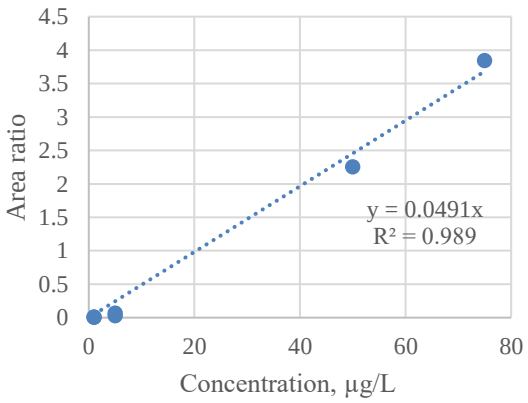
Tetracycline
Area ratio
Concentration, µg/L
y = 0.0491x
R² = 0.989
0
0.5
1
1.5
2
2.5
3
3.5
4
4.5
0
20
40
60
80

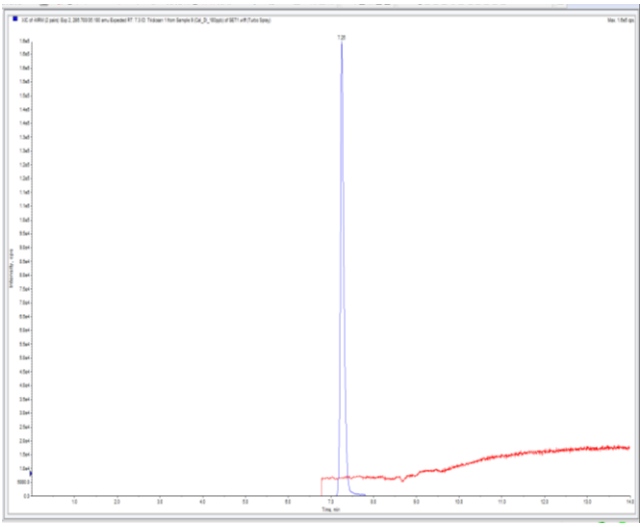

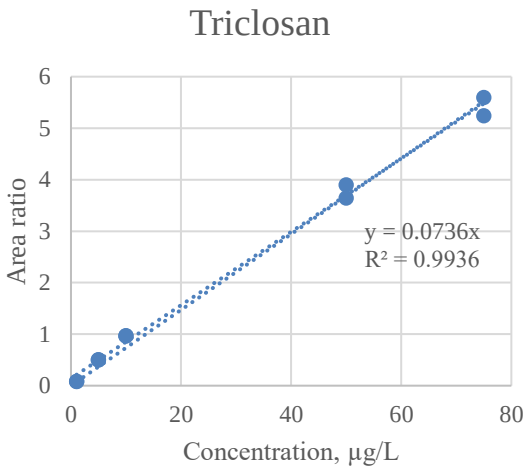
Triclosan
Area ratio
Concentration, µg/L
y = 0.0736x
R² = 0.9936
0
1
2
3
4
5
6
0
20
40
60
80